JPL PUBLICATION 79-69, REVISION 1

Evaluation of the JPL X-Band 32-Element Active Array

Final Report

J. F. Boreham
R. B. Postal
B. L. Conroy

August 1, 1979

Prepared for
U. S. Air Force Space and Missile Systems Organization
by
Jet Propulsion Laboratory
California Institute of Technology
Pasadena, California

ABSTRACT

The report describes a number of tests performed on an X-band 32-element active array developed at JPL under a NASA-sponsored project and evaluated with funding from the U.S. Air Force Space and Missile Systems Organization. Antenna pattern characteristics of the array were tested in its standard operating mode as well as several degraded performance modes, including failures of 1, 2, 3, 4, 8, 16, and 31 elements. Additionally, the array was characterized with the addition of a metallic shroud, and also characterized versus rf drive level and at a single off-axis electronic beamsteered position. Characterization was performed on several of the 3/4-watt, three-stage, X-band solid-state power amplifier modules. The characterization included swept amplitude response, amplitude and phase versus temperature from -20 to +60°C, and intermodulation distortion of selected modules. The report includes a description of the array as well as conclusions and recommendations based upon the experience and results achieved in performance of this project.

DEFINITION OF ABBREVIATIONS AND SYMBOLS

AFAL	Air Force Avionics Laboratory
AFPA	array feed power amplifier
DUT	device under test
ERP_a	calculated array radiated power
ERP'_a	measured array effective radiated power
F_a	array factor
FET	field-effect transistor
f_o	center frequency
G_{ala}	measured array gain without amplifiers
G_{amps}	measured gain of 32 amplifier modules
G_e	element gain
G_h	standard horn gain
G_t	expected active array gain
G_{tm}	measured active array gain
HP	Hewlett-Packard
IMD	intermodulation distortion
P_t	total power of all modules
P_h	power level at the horn
rf	radio frequency
S/N	Serial Number
SAMSO	U.S. Air Force Space and Missiles Systems Organization
TWTA	traveling wave tube amplifier
η_a	array aperture efficiency
η_{PA}	power added efficiency
ΔP_r	difference in received power between horn and array

CONTENTS

APPENDIXES

Figures

Tables

ACKNOWLEDGEMENTS

The authors would like to acknowledge the contributions of Mr. Donald Yenche and Mr. Denman Hyett who obtained the data for this report. They would also like to thank Mr. Robert Thomas and Mr. Gilbert Voyles for their assistance in making the radiation patterns.

SECTION 1

INTRODUCTION AND BACKGROUND

1.1 INTRODUCTION

This final technical report summarizes the details and results of the 32-Element X-Band Active Array Project performed for the United States Air Force Space and Missile Systems Organization (SAMSO) by the Jet Propulsion Laboratory under an agreement between the National Aeronautics and Space Administration and SAMSO (Appendix A). The report includes conclusions and recommendations based upon the experience and results achieved in performance of the project.

NASA, through JPL, has for some time recognized the need for the development of solid-state replacements for the expensive, life-limiting TWTAs currently used as the final rf amplifier at X-band on deep space missions, and has funded such a program through RTOP 506-20-45 over the last three years. The first phase of this effort culminated in October 1978 in the successful demonstration of 25 watts of X-band rf power injected into the radiating elements of a 32-element phased array, which, for deep space purposes, will be used as a near field Cassegrainian feed system for a large parabolic dish. The Air Force, through the Space and Missile Systems Organization (SAMSO), the Air Force Avionics Laboratory (AFAL), and the Aerospace Corporation, has also recognized the need for solid-state microwave amplifiers for some time as evidenced by a 1975 Aerospace Corporation report for the Military Satellite Communications Office of the Defense Communications Agency, TOR-0076-(6792)-1, Vol. I, Nov. 75, encompassing military, commercial, and NASA ComSat programs from 1963 to 1975.

For Air Force usage, the array could be used as stated above if high ERP is the objective or as a stand alone antenna if the application is beamwidth limited. Further applications include beamsteering through the inclusion of phase shifters and a control system, or to enable a high data rate through the addition of higher power output from each amplifier.

1.2 REPORT ORGANIZATION

This section describes the basics of the JPL X-band 32-element array antenna. Section 2 describes the tests made on the individual amplifier modules of the array, while Section 3 summarizes the radiation tests performed on the assembled array. Section 4 discusses the conclusions derived from the tests. Recommendations for future improvements of solid-state amplifiers and array antennas are in Section 5. Due to the large volume of test data (patterns, temperature runs, bandwidth plots, etc.) taken during the course of this project, the data is only summarized in this report.

1.3 PHASED ARRAY AND AMPLIFIER DESCRIPTION

Figure 1-1 shows the assembled 32-element X-band active phased array with its component parts identified. Figure 1-2 is a block diagram of the signal flow through the array. A four-way divider feeds four eight-way dividers, which feed the externally adjustable phase shifters, which feed the amplifier modules, which feed the radiating elements. Since all the signals radiated by the elements are essentially in-phase, they recombine in free space in the array aperture. The far field active array beamwidth is 4.3 degrees.

A condensed description of the array and its application as a feed for a larger parabolic antenna was presented at the IEEE International Symposium on Antennas and Propagation in June 1979 and is included in Appendix B.

A more detailed view of the amplifier assembly is shown in Figures 1-3 and 1-4. A three-bit, hard-wired, phase shifter, located between the first and second stages, was designed to provide coarse phasing of the units during final test. The peak-to-peak spread of 36 units manufactured was such that it was only necessary to use the least bit on two modules.

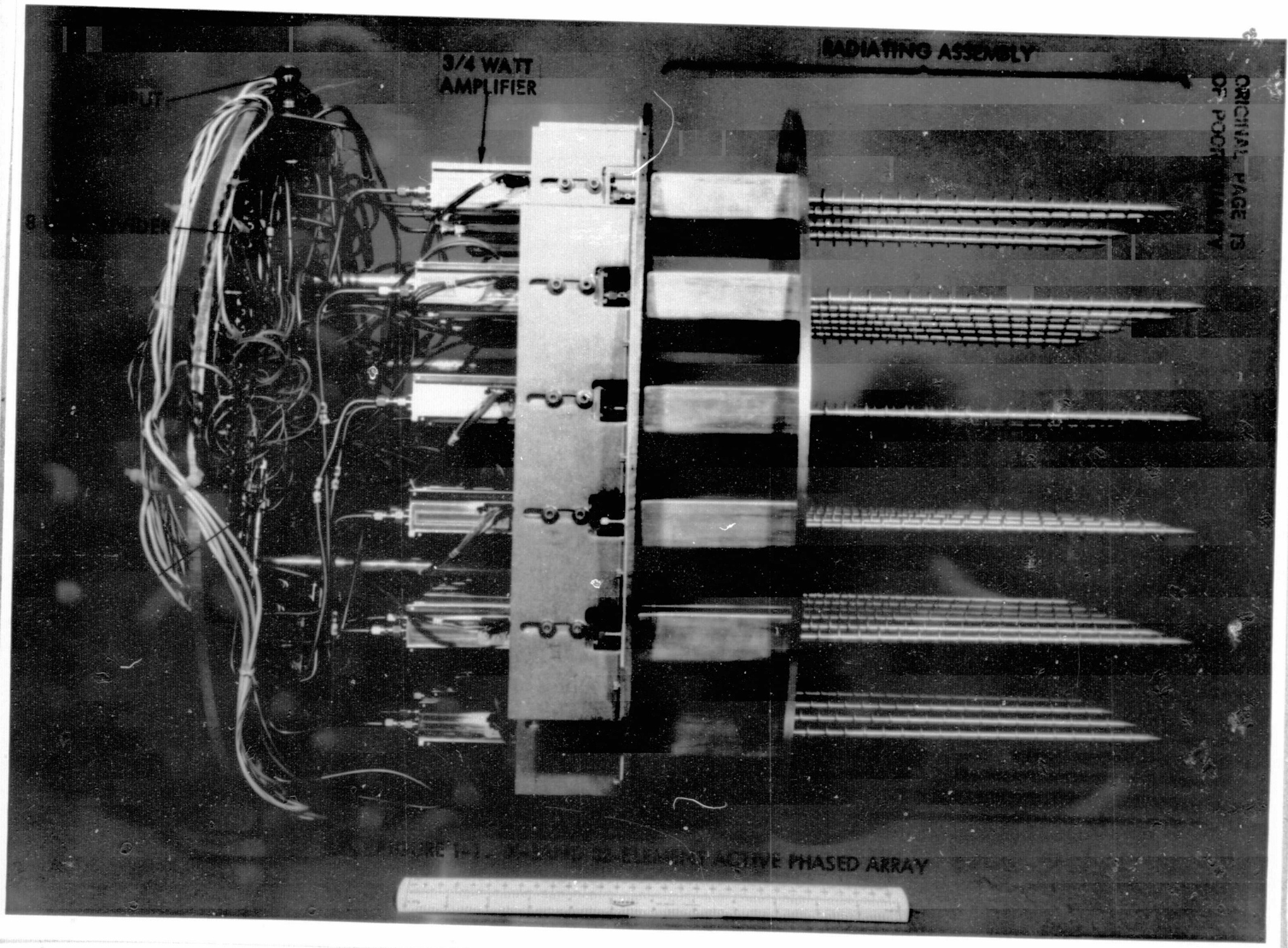

ORIGINAL PAGE IS
OF POOR QUALITY

FIGURE 1-1 ... ELEMENT ACTIVE PHASED ARRAY

SECTION 2

AMPLIFIER ELECTRICAL TESTS

2.1 AMPLIFIER TEST OBJECTIVES

The objectives of the amplifier test program (Appendix A) were to measure, evaluate, and minimize phase and amplitude sensitivities of 10 modules through compensation for temperature over a range of -20 to +50°C. Because the JPL usage was narrowband and emphasized optimum performance at only the center frequency, all 32 modules were measured for bandwidth to select 10 wideband candidates for the temperature tests. Two additional modules were included for a total test sample of 12 units, and the upper temperature test limit was increased to 60°C.

The original objective of module temperature compensation was assessed only on a theoretical basis because the measured results indicated a high degree of unit-to-unit tracking over the temperature range. Additional tests regarding amplifier transfer characteristics were substituted for the phase compensation task to compare phase, amplitude, and distortion performance over both linear and compressed drive conditions.

2.2 TEST PROCEDURE/METHODOLOGY

The amplifier modules were individually tested in the following order:

Test	Units Tested	Report Subsection
Rf bandwidth at 25°C, from 8 to 9 GHz	32	2.3
Phase and amplitude, $f_o \pm 200$ MHz vs. temp.	12	2.4
Transfer characteristics	6	2.5

Based on the bandwidth plots, 12 candidate amplifier modules were selected for amplitude and phase testing over a temperature range of -20 to +60°C. Selection criteria included bandwidth symmetry about 8415 MHz (f_o) and minimum drop-off at $f_o \pm 200$ MHz. Six of the twelve units were then selected at random for evaluation of rf transfer characteristics.

A block diagram showing the test configuration for the bandwidth and temperature tests is illustrated in Figure 2-1. Chamber temperature, input frequency, and data plotting and storage are automatically controlled by a Hewlett-Packard (HP) 9830 calculator. The network analyzers provide module output phase and amplitude measurements, as well as monitoring of its input impedance. A calibrated reference line is contained within the temperature chamber to allow for system phase and amplitude tracking. Calibration of system errors over a temperature range of -20 to +60°C indicates phase and amplitude tracking errors to be within 2 degrees and 0.1 dB, respectively.

For the bandwidth tests, the frequency was stepped from 8 to 9 GHz in 2.5-MHz increments. System calibration data were taken at each frequency and stored in the controller for correction of the actual data. This technique gave an accuracy of ±0.05 dB over the entire frequency range; however, the device under test (DUT) introduced a standing wave in the system, which resulted in some uncompensated ripple.

In the temperature test, each test consisted of a full temperature cycle starting at room temperature, going to the high limit (60°C), going to the low limit (-20°C), and then returning to room temperature. Rate of temperature change was maintained at 1 degree per minute. At each degree change, phase and amplitude data at each of five frequencies (f_o, ±100 MHz, ±200 MHz) were taken and stored on magnetic tape.

The system plotted out the center frequency data in real time so the operator could check for proper operation. The real-time raw data show two undesirable effects: temperature hysteresis and small jumps in amplitude and phase. The hysteresis appears to be substantially due to a physical effect in the substrate material because further decreases in the rate of temperature change do not reduce it appreciably. To compare the unit-to-unit differences in a consistent manner, all modules were evaluated and compared on the basis of the continuous downward temperature run. The small jumps in the data are inherent in a digitally sampled system. The sample is taken at a particular instant of time and may be affected by any short duration noise, such as line transients. To filter out this effect, each data point was averaged with the two adjacent points in a data reduction program.

2.3 AMPLIFIER RADIO FREQUENCY BANDWIDTH TEST RESULTS

Test results for the rf bandwidth measurements of the 32 amplifier modules indicate the mean 1-dB bandwidth relative to 8415 MHz to be 443 MHz with a median value of 450 MHz. Three bandwidth plots typical of the 12 units selected for temperature tests are shown in Figure 2-2. All modules were designed, aligned, and tested for operation at +13 dBm input. The narrower bandwidth and center frequency shifts at the +3 dBm drive level are typical of a saturated amplifier being operated in a linear mode.

2.4 AMPLIFIER TEMPERATURE TEST RESULTS

Typical real-time, raw data at 8415 MHz (f_o) of module S/N 23 is given in Figure 2-3. As shown, amplitude and phase variations are within the specification limit of 1 dB and 20 degrees, respectively, over the temperature range of -20 to +50°C.

The high phase slope that occurs near room temperature is typical of all units but is still unexplained and is further discussed in Section 4.

Module S/N 23 performance at $f_o \pm 100$ MHz is shown in Figure 2-4. This plot is taken from magnetically stored information and presented in the data reduction format (see subsection 2.2).

Comparable plots for all 10 amplifier modules taken at f_o ±200 MHz are given in Figure 2-5. Statistical phase information of the 12 modules is shown in Figure 2-6 for each of the five test frequencies. As indicated, the mean phase excursion due to temperature for the 12 modules range between 20 and 24 degrees. For each frequency plot, the upper dashed line represents the effects of theoretical linear phase compensation of each module. A linear compensating slope was computed for the f_o of each module, and this compensating slope was subtracted from the slope of each frequency. Compensation slopes ranged roughly from -1/4 to -1/2 degree per degree Celsius. This could, if physically realizable, reduce the mean phase excursion to a maximum of 12 degrees.

Of even more significance, the bottom half of each figure shows the phase standard deviation of the 12 units tested along with the calculated linear phase-compensated (at 8415 MHz) results. Based on these results, it was mutually agreed between SAMSO and this research group that phase compensation to achieve the specification level of ±10 degrees one sigma could be easily accomplished; hence, the tests described in subsection 2.5 were substituted for that task. It is also significant to note that the high slope transition near room temperature does not increase the standard deviation in that region, which indicates a high degree of unit-to-unit similarity of this feature.

2.5 AMPLIFIER TRANSFER CHARACTERISTICS

This subsection addresses amplifier performance characteristics at room temperature versus input drive level. For six selected modules, output amplitude, phase, and third-order intermodulation distortion (IMD) were measured. Power-added efficiency (η_{PA}) was also calculated.

A block diagram of the test set for amplitude measurements is illustrated in Figure 2-7. Phase measurements were performed with the test set shown in Figure 2-1.

The IMD tests were performed using two equal-amplitude carriers spaced 10-MHz apart with a mean frequency of 8415 MHz. Output products at 10-MHz intervals above and below the input frequencies are due to a cubic term in the transfer function, and their level is called the third-order intermodulation distortion. The output amplitude characteristics for the six modules are shown in Figure 2-8. A summary of the fundamental performance data is listed in Table 2-1. Table 2-2 shows the third-order distortion data, while Table 2-3 presents the phase deviation versus drive relative to the +13-dBm operating point.

Table 2-1. Amplifier Fundamental Carrier Characteristics

Module S/N	Saturated Performance P_{in} = +13 dBm: RF Output Level, dBm	Saturated Performance P_{in} = +13 dBm: η_{PA}, %	Levels for 1-dB Compression: Input, dBm	Levels for 1-dB Compression: Output, dBm
5	28.8	27.0	5.5	27.4
7	28.4	27.2	8.0	27.2
17	28.5	26.3	6.6	26.0
20	28.8	30.6	3.8	26.8
23	28.5	26.7	5.0	27.6
26	28.5	26.7	4.0	26.0

Table 2-2. Amplifier Intermodulation Distortion Characteristics

Module S/N	IMD Level, Output Backed Off 3 dB, dB	Output Level, for IMD = -20 dB, dBm	Intercept[a] Point, dBm
5	-23.0	27.0	35.7
7	-23.2	26.4	38.4
17	-22.5	26.4	38.2
20	-21.5	26.6	38.0
23	-25.0	27.0	36.8
26	-22.0	26.0	36.4

[a]Output level at which the projections of the fundamental and third-order outputs intersect.

Table 2-3. Amplifier RF Phase vs Drive Sensitivity

RF Input Level, dBm	Relative RF Phase, Deg					
	S/N 5	S/N 7	S/N 17	S/N 20	S/N 23	S/N 26
+14	- 4.0	-10.0	-0.5	- 4.0	- 2.0	- 2.0
+13	0	0	0	0	0	0
+12	+ 4.5	+ 9.0	+0.7	+ 4.0	+ 2.0	+ 4.0
+11	+ 8.5	+13.0	+1.0	+ 6.5	+ 3.5	+ 8.5
+10	+10.0	+15.5	+2.5	+ 9.5	+ 4.5	+13.0
+ 5	+ 9.0	+16.5	+3.0	+18.5	+12.5	+24.0
0	+ 8.0	+13.0	+1.0	+16.5	+12.0	+23.0
- 5	+4.0	+ 9.0	-2.0	+12.5	+ 8.5	+19.5

SECTION 3

ARRAY PATTERN TESTS

3.1 ARRAY PATTERN TEST OBJECTIVES

The objectives under this subsection were to perform antenna range measurements of the array radiation patterns ±30 degrees from boresight and peak gain for a normal operating mode. Similar patterns for a number of selected single and multiple-element failure modes and peak gain degradation were of prime interest. These and additional tests (including rf drive effects, single-element patterns, and a special reflective shield test) were performed in JPL's 18.3-meter (60-foot) anechoic range facility.

3.2 ARRAY TEST PROCEDURE/METHODOLOGY

In preparation for array pattern tests, all components of the array except the 32 radiating elements were assembled. Electrical phasing and calibration of the individual amplifier modules were performed. Relative phase of all amplifiers was adjusted to within ±5 degrees, and output levels were measured to be within ±0.25 dB. The standard deviation of the 32-element phasing was 2.5 degrees. Because of the mechanical symmetry of the radiating elements, they were assumed to be equi-phased.

The radiating assembly was then attached, and the complete array was checked out and installed in JPL's anechoic test facility. The array, mounted on an antenna positioner roll head, is shown in Figure 3-1. Also shown is a standard gain horn diametrically situated with the array to provide a gain reference.

A block diagram of the system test equipment for the antenna range measurements is shown in Figure 3-2. Input drive to the horn and array is fed from the array test set through a calibrated switch and transmission line assembly. A precision attenuator at the receiver input provides an accurate means of measuring the differential gain between the array and standard gain horn. The receiver output is plotted on a Scientific Atlanta analog strip chart recorder. System measurement accuracies are summarized in Table 3-1.

The array test set provides dc power, instrumentation for the array, and rf drive for the horn/array assembly. The 85 watts of dc drain circuit power for the array are furnished by four separate power supplies, each powering a quadrant of eight amplifier modules. A gate circuit dc bias power of 1.5 watts for all amplifiers is derived from a single power supply. Several telemetry monitoring points at the array allow for precise setting of amplifier operating voltages as well as the monitoring of operating temperatures of two selected amplifier modules.

The array test set and array (operating in a laboratory test configuration) are shown in Figure 3-3. The instrument shown under the table in Figure 3-3 is an rf snooper used for electromagnetic radiation hazard measurements. For personnel safety, the snooper was used each time

the array was set up because power density near the array aperture is estimated to be as high as 25 mW/cm^2.

Pattern tests were performed in the standard array configuration (normal operating mode) and for a number of selected element failure modes. Element failures were accomplished by disconnecting dc power from the appropriate amplifier modules which simulates the most probable catastrophic failure mode. Pattern tests for each configuration consist of a ±30-degree azimuth (cone angle) scan for each of eight roll (clock) angles from 0 to 90 degrees in 15-degree increments with an additional pattern at an angle of 135 degrees.

3.3 ARRAY GAIN AND APERTURE EFFICIENCY

Because the array is active (that is, producing gain), the normal antenna gain measurement by substitution of a standard gain horn must be modified. The theoretical array effective radiated power (ERP_a) can be obtained through the knowledge of the total rf power supplied by the 32 array amplifiers (P_t), the average measured element gain (G_e) (the five unique element gains were used), and the 32-element array factor F_a (15.05 dB) through the following relationship:

$$ERP_a = P_t \cdot G_e \cdot F_a \qquad (1)$$

This will be modified by the array grating lobes and the amplitude imbalances and phase errors of the radiating system, which collectively are defined as the array aperture efficiency (η_a) such that

$$\eta_a = ERP'_a/ERP_a \qquad (2)$$

where ERP'_a is measured by the standard gain horn substitution method, and

$$ERP'_a = P_h \cdot G_h \cdot \Delta P_r \qquad (3)$$

where P_h is the power level at the horn, G_h is the horn gain and ΔP_r is the difference in received power between the horn and the array.

During the measurement process, the following values were obtained:

P_t = 43.58 dBm P_h = 30.5 dBm

G_e = 15.17 dB G_h = 15.03 dB

ΔP_r = 27.8 dB

and, from equations (1) and (3):

ERP_a = 73.80 dBm and ERP'_a = 73.33 dBm

Hence, from equation (2), the calculated aperture efficiency is 89.7%.

Similarly, from a prior measurement of the array gain made without the amplifiers (G_{ala}) and the average measured gain of the 32 amplifier modules (G_{amps}), the overall expected active array gain (G_t) was calculated to be:

G_{ala} = 27.35 dB

G_{amps} = 15.53 dB

G_t = 42.88 dB

This compares very well with the measured active array gain (G_{tm}) calculated from ΔP_r and G_h of 42.83 dB.

3.4 ARRAY PATTERN TEST RESULTS

This subsection addresses radiation pattern test results for the standard array configuration as well as for a variety of failure mode combinations. A list of failure modes tested is given in Table 3-2. Figure 3-4 illustrates the array configuration as viewed from the receiving horn antenna.

All eight of the standard array patterns are shown in Figure 3-5. Due to the large number of patterns taken, only one set of two patterns (roll = 0 and 45 degrees) is shown for each failure category; however, all test results are recorded in the tables, and detailed results are available on microfilm for future reference.

Although there are 32 amplifier modules, it is possible to show the effect of any single failure by testing only 5 single-module failures because of array symmetry. A sample single-module failure is shown in Figure 3-6. The main lobe degradation is shown to the right of the lobe on each failure mode pattern. The results of all five single-module failures are listed in Table 3-3.

Due to the large number of combinations of multiple-element failures, not all combinations could be examined. Typical examples of patterns for two, three, and four unpowered modules are shown in Figures 3-7 through 3-9, and Tables 3-4 and 3-5 summarize the main lobe degradation of all the failure modes that were examined. Figure 3-10 shows patterns representing the outer 16 modules unpowered (unexpected results derived from data in Figure 3-10 are discussed in subsection 3.5). Figure 3-11 shows the array patterns with one quadrant unpowered. Figure 3-12 shows array pattern performance with three quadrants unpowered. Table 3-6 summarizes these and other 8-, 16-, and 24-element failure modes tested.

A comparison of the gain degradation of several of the failure modes discussed above, with the expected values[1] (calculated from software developed under NASA sponsorship) is shown in Table 3-7.

Single-element pattern tests were performed, in the array, on the five unique elements. The patterns given in Figure 3-13 show element B1 performance in the presence of 31 unpowered elements. These patterns were taken to aid in the assessment of the array aperture efficiency and to assess the errors introduced by using free space element patterns in the generation of computer-calculated array feed/reflector secondary patterns.

To see the effects of beamsteering, the phase shifter for each module was readjusted to produce a phase slope across the array of -40 to +40 electrical degrees in the E-plane. The 80-degree slope represents a beam shift goal of 1/3 beamwidth. A larger beam shift was not attempted because of mechanical travel limitations in the external phase shifters. Figure 3-14 shows the resulting beam shift of -1.26 degrees in the E-plane. The calculated value for this phase slope is -1.27 degrees.

Rf input power to the array was varied to assess pattern effects caused by amplifier phase and amplitude variations with drive. A comparison of both normal and -5 dB drive patterns for the E-plane are also presented in Figure 3-14. As shown, the array signal pattern changed very little other than a 1.0-dB decrease in amplitude produced by the 5-dB reduction in input drive level. On a module test basis (sample of 12) a comparable input level reduction produced an average output loss of 0.76 dB. The additional 0.24-dB loss in the array measurement is attributed to element amplitude and phase imbalance at the lower drive level.

---

[1]Per private communications with Dr. Kenneth Woo from data to be published.

3.5 SHIELDING EXPERIMENT/UNDEFINED OUTPUT ENHANCEMENT TEST

In the case of the 16-element failure (shown in Figure 3-10), it was noticed that the main lobe beamwidth increased more than the gain decreased. An improvement in array performance of 0.8 dB was calculated. One explanation is that the 16 unpowered outer elements were presenting a better impedance match to the 16 active inner elements, thereby appearing electrically as an infinite array to the active elements. It was theorized, therefore, that an aluminum shield placed one wavelength away from the active array would also improve array performance.

Tests were then performed with the full array on for several shield lengths. Best results showed an improvement of only 0.2 dB for a shield length measured from the ground plane of 27.2 cm (10.7 in.). A sample of patterns for the shield test is given in Figure 3-15.

3.6 ARRAY AMPLIFIER EFFICIENCY

On initial assembly of the array, the total rf power output was 25.13 watts. The dc power required was 88.63 watts, and the rf drive power was 1.11 watts. Thus the power added efficiency of the array was 27.1%. After 125 hours of operation, the total rf power output was 22.09 watts, and the dc power was 77.96 watts, yielding a power added efficiency of 26.9%. From the 125 hours of operation to present (about 1300 hours of operation), no significant drift has been observed. It is believed that the initial drift observed would have been avoided if the devices had been burned in before the construction of the modules.

Table 3-1. Pattern Test System Accuracies

System Function	Measurement Error
Electrical and mechanical boresight	0.2 deg RMS
Electromechanical synchro positioner	0.1 deg
Plotter amplitude readout (strong signal)	0.05 dB
Plotter amplitude readout (-30 dB)	0.25 dB
Horn/array input level settability	0.15 dB

Table 3-2. Failure Mode Tests Performed

Number of Elements Off	Number of Tests	Number of Elements Off	Number of Tests
1	5	Outer 16	1
2	12	1 quadrant (8)	4
3	4	2 quadrants (16)	2
4	3	3 quadrants (24)	1

Table 3-3. One-Element Failure

Elements Off	Peak Location		Gain Degradation, dB
	Cone Angle, Deg	Clock Angle, Deg	
A1	0	0	-0.2
A2	-0.05	82	-0.3
A3	0	0	-0.3
A4	-0.25	42	-0.4
A5	-0.1	60	-0.2

Table 3-4. Two-Element Failure

Elements Off	Peak Location		Gain Degradation, dB	Elements Off	Peak Location		Gain Degradation, dB
	Cone Angle, Deg	Clock Angle, Deg			Cone Angle, Deg	Clock Angle, Deg	
A1, A2	-0.25	22	-0.5	A3, D3	-0.1	82	-0.5
A1, A3	0	0	-0.55	A5, D5	-0.15	52	-0.5
A2, A3	-0.15	45	-0.6	A1, D8	-0.3	45	-0.55
A2, A4	+0.1	60	-0.6	A2, C2	0	0	-0.6
A2, A5	0	0	-0.6	A1, C1	-0.3	37	-0.55
				A5, C5	-0.1	75	-0.5
				A3, C3	0	0	-0.65

Table 3-5. Three- and Four-Element Failures

Elements Off	Peak Location		Gain Degradation, dB
	Cone Angle, Deg	Clock Angle, Deg	
A2, A3, A6	0	0	-1.0
B3, B4, B5	-0.1	30	-0.8
A3, C3, D3	0	30	-0.9
A5, C5, D5	0	45	-0.85
A1, B1, C1, D1	-0.25	82	-1.15
A5, B5, C5, D5	0	0	-1.3
A3, B3, C3, D3	-0.1	15	-1.3

Table 3-6. 8-, 16-, and 24-Element Failures

Elements Off	Peak Location		Gain Degradation, dB
	Cone Angle, Deg	Clock Angle, Deg	
Quad A	-0.05	0	-2.8
Quad B	+0.1	0	-2.7
Quad C	-0.15	0	-2.0
Quad D	-0.4	0	-2.7
Outer 16	0	90	-5.55
Inner 16	-0.25	60	-6.3
Quads A, B	+0.7	90	-6.5
Quads B, D	0	75	-6.4
Quads A, B, D	-2.5	90	-13.4

Table 3-7. Gain Degradation Calculated vs Measured

Configuration		Gain Degradation		
No. of Elements Off	Elements Off	Calculated, dB	Measured, dB	Delta, dB
1	A2	-0.26	-0.3	-0.04
2	A1, D8	-0.55	-0.55	0.00
3	A5, C5, D5	-0.81	-0.85	-0.04
4	A5, B5, C5, D5	-1.10	-1.3	-0.20
8	Quad A	-2.48	-2.8	-0.32
16	Outer 16	-6.00	-5.6	+0.40

SECTION 4

CONCLUSIONS

This section summarizes the significant findings and conclusions generated during the course of the testing program.

In general, the AFPA has been shown to be an effective method for combining the outputs of many solid-state amplifiers. The AFPA design configuration allowed:

(1) Ease of system assembly

(2) Ease of phasing and testing of the individual amplifier outputs

(3) Simplicity in failure mode simulations. For amplifier removal and retrofit, however, a turnaround time of six hours was required.

Concerning amplifier phase and amplitude stabilities, it is apparent that the module-to-module temperature tracking is consistent enough for the phased array application. Additional margin may be gained with simple linear compensation.

The cause of the high-phase slope that occurs near room temperature is being investigated. However, the slope location and form is typical of all modules tested. Possible causes of the phase anomaly include:

(1) Generic GaAs field-effect transistor (FET) device or circuit idiosyncrasy

(2) Chassis wave guide moding

(3) Module alignment temperature

Also, this phenomenon has been observed at JPL in previous tests of a different vendor (RCA) GaAs FET device in a test fixture.

For the array performance, the AFPA aperture efficiency has been shown to be nearly 90%, which is typical for a well designed non-active phased array. Efficiency of the radiating elements, however, appears to be lower than expected, probably due to excessive dielectric losses and launcher mismatches.

The relative antenna patterns before and after insertion of the amplifiers into the feed assembly were virtually identical when the amplitude and phase distributions of the signals feeding into the array elements were correctly adjusted.

SECTION 5

RECOMMENDATIONS

Development of solid-state replacements for TWTAs should continue on three major approaches:

(A) Basic device reliability and device improvements

(B) AFPAs and their derivatives

(C) TWTA "drop in" replacements

Regarding device reliability approach, the following is recommended:

(1) Conduct a life test of 24 of the 3/4-watt modules, under rf drive and at the high type approval temperature limit (75°C) for at least one year.

(2) Enter a contract with the GaAs FET manufacturer to improve the power-added efficiency of the devices into the 40% range through device design improvements as well as internal matching. All design changes will be evaluated for their effects on reliability.

(3) Investigate and understand the phase anomaly near room temperature.

Future AFPA work should include the following:

(4) Improve launcher and element design.

(5) Develop a more compact module for weight reduction with a final solution to conducting the dissipative heat to a radiating surface. The latter is important to set the derating factors for the GaAs FET operating points.

(6) Design a fine-phase adjuster (±45°) that can be electrically set and possibly commanded. This component would be integrated into the amplifier module to facilitate phase alignment of the array during assembly and would replace both the externally adjustable phase shifter and the three-bit hard-wired phase shifter.

(7) Design a unitized 32-way power splitter to replace the four-way and eight-way splitter network.

(8) Design a redundant, high-efficiency, fail-safe, dc-dc power converter to supply the array.

(9) Extend the phase shifter capability to a full 360 degrees to allow a beamsteering capability with the use of an appropriate controller.

(10) Investigate the use of more radiating elements for high reliability and/or higher power.

In the area of TWTA replacements, the following is recommended:

(11) Develop a higher power output capability in the 1.5- to 3-watt range to reduce the number of paralleled amplifiers required so that output transmission line combiner losses may be minimized. These higher power modules could also be used in the AFPA to produce a higher ERP with the same number of elements or the same ERP with fewer elements.

(12) Develop a highly efficient output power combiner (greater than 90% goal).

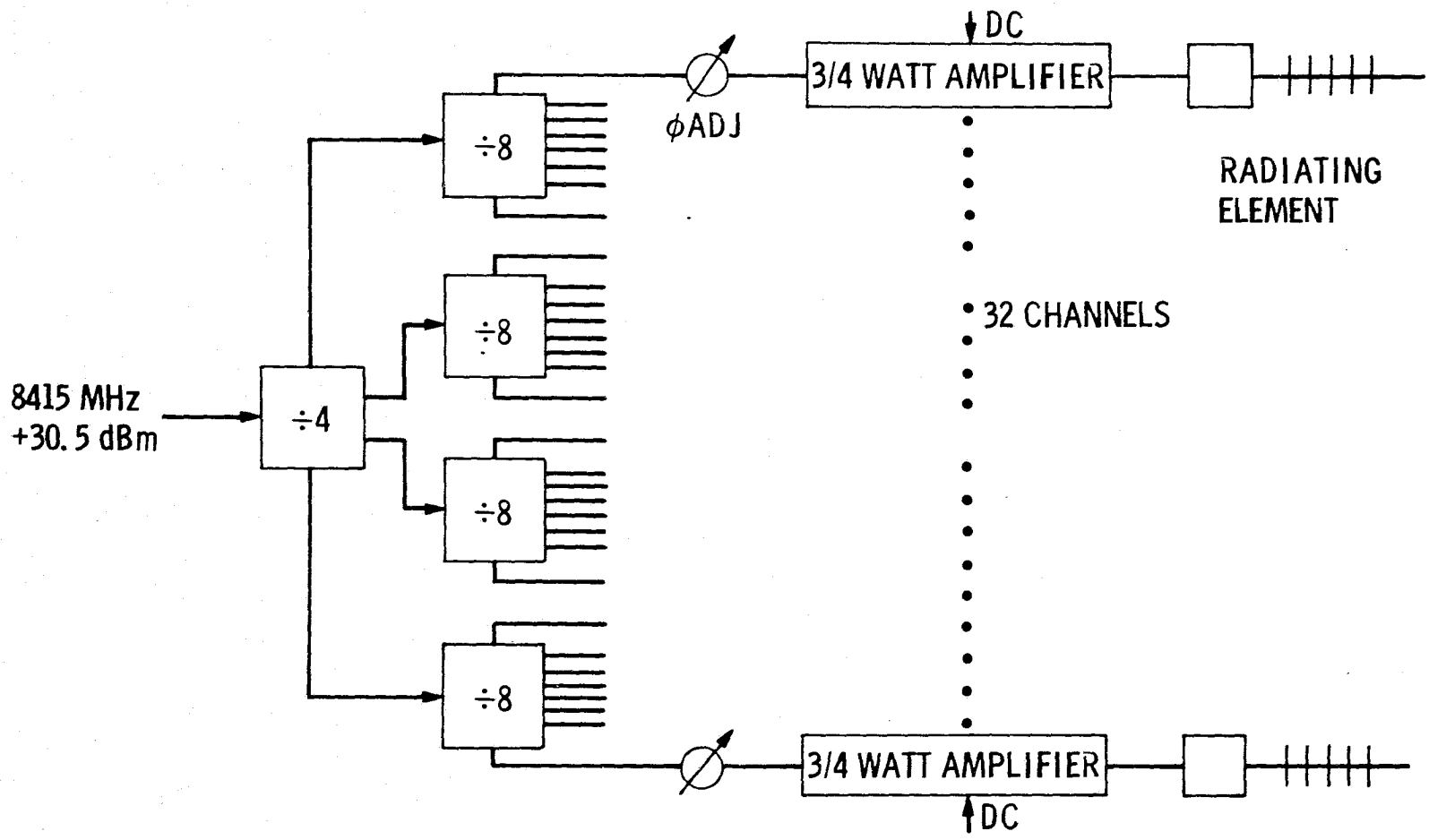

Figure 1-2. X-Band Array Block Diagram

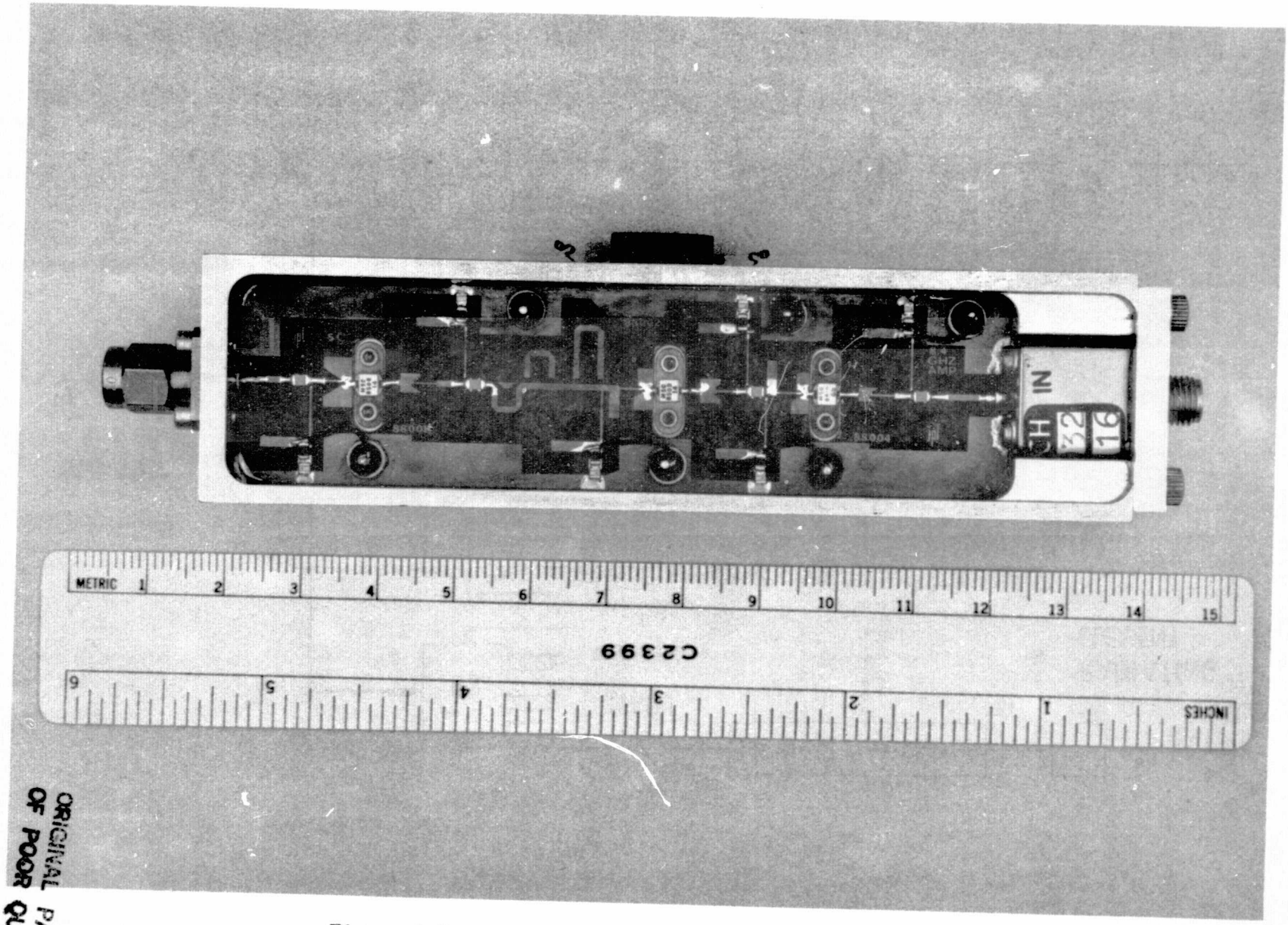

Figure 1-3. X-Band Amplifier Module With Cover Off

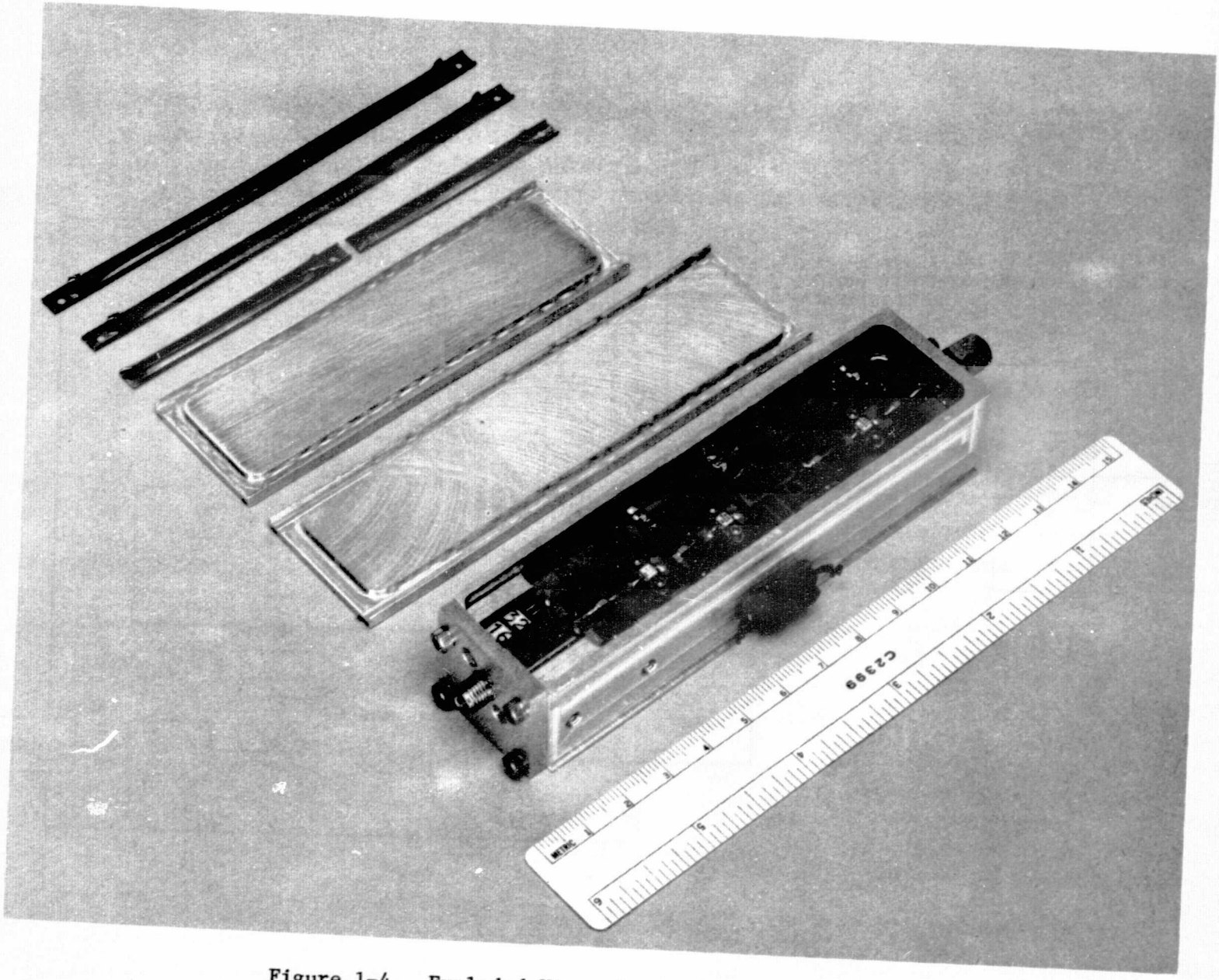

Figure 1-4. Exploded View of X-Band Amplifier Module

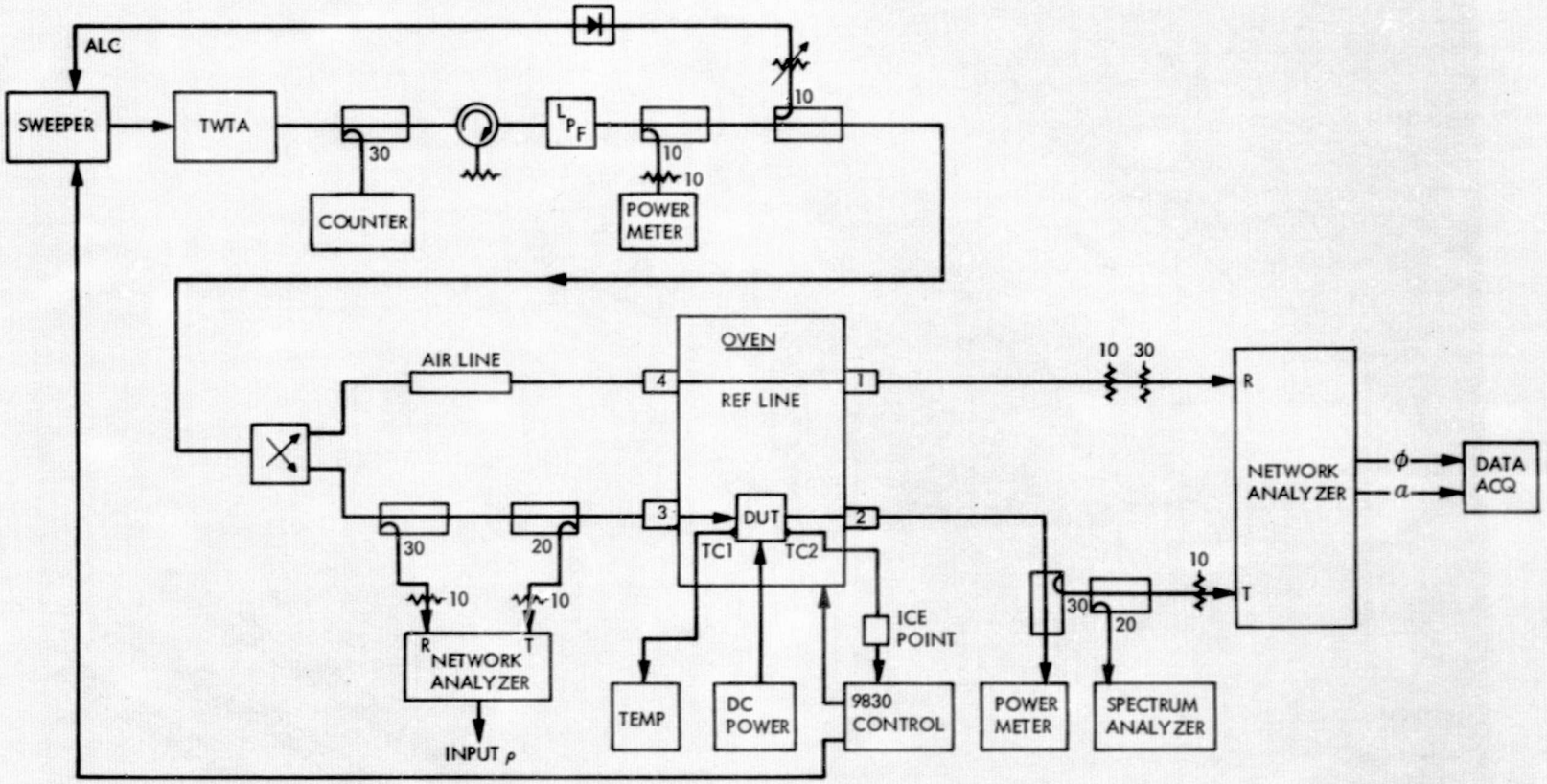

Figure 2-1. X-Band Automatic Control and Data Acquisition Test Set

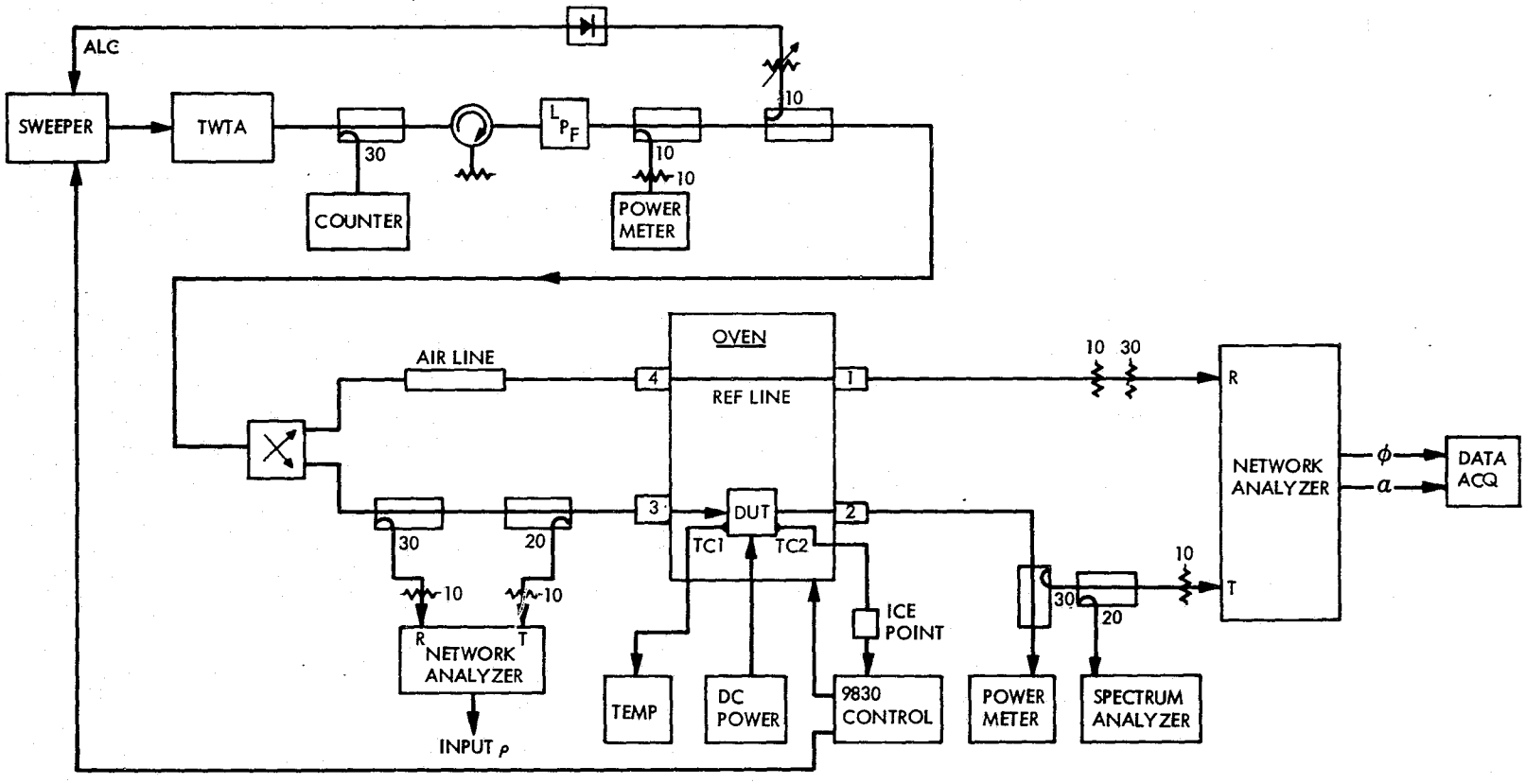

Figure 2-1. X-Band Automatic Control and Data Acquisition Test Set

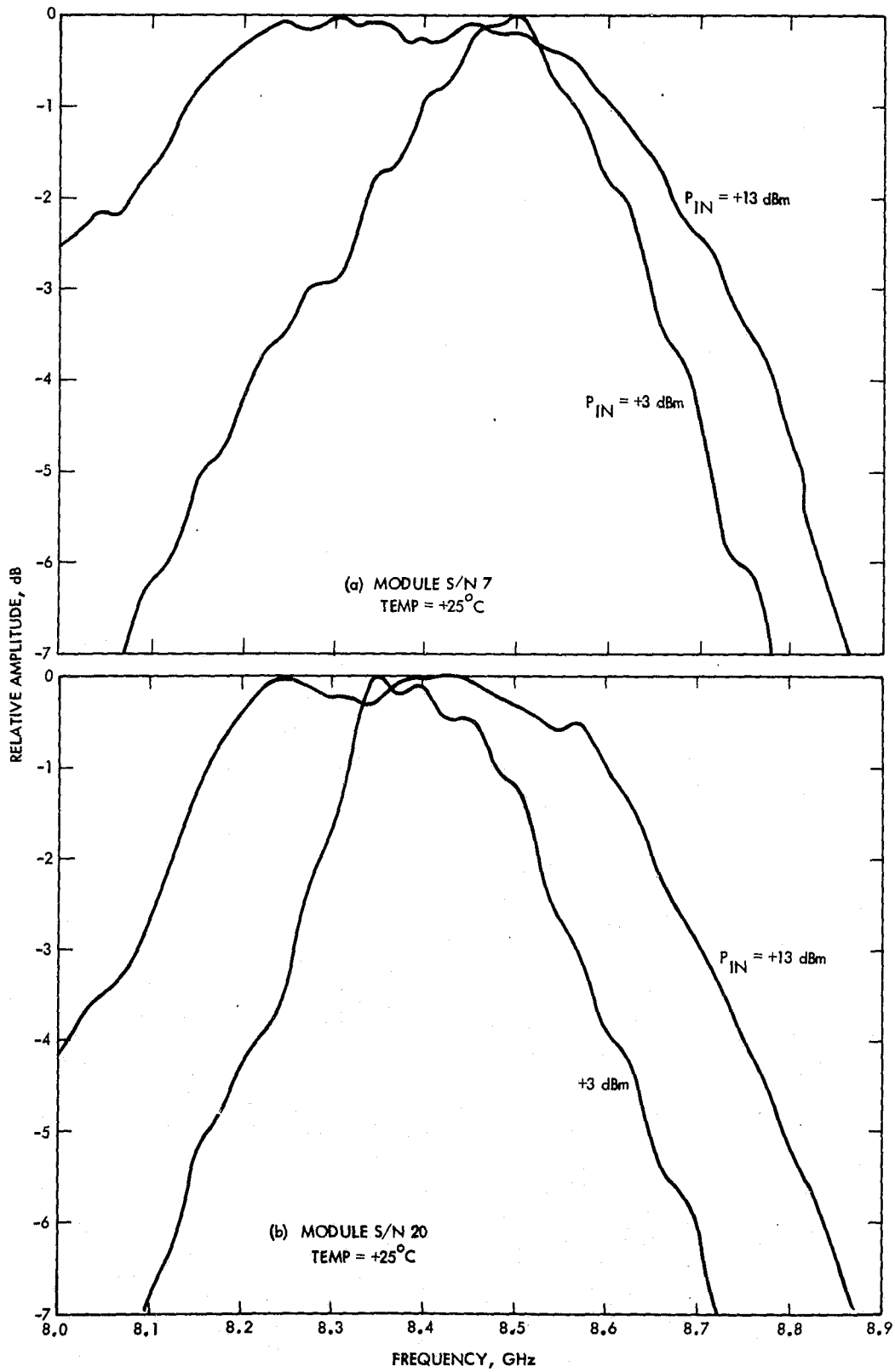

Figure 2-2. Relative Amplitude Versus Frequency

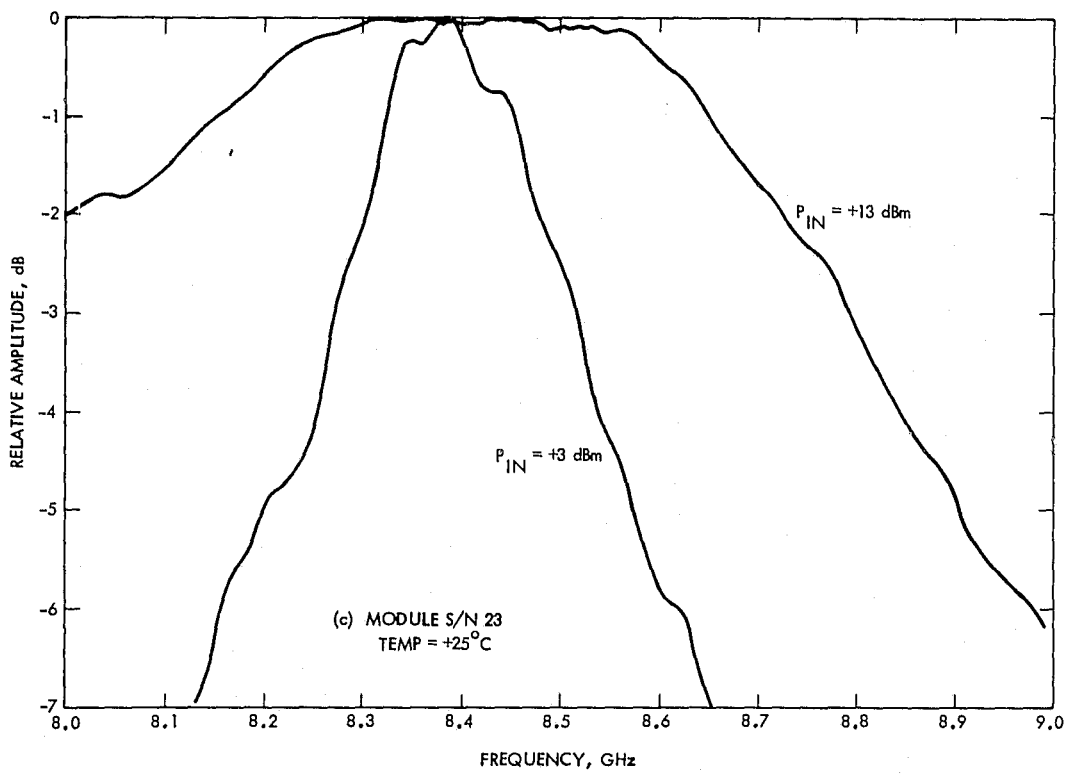

Figure 2-2. Relative Amplitude Versus Frequency (Continuation 1)

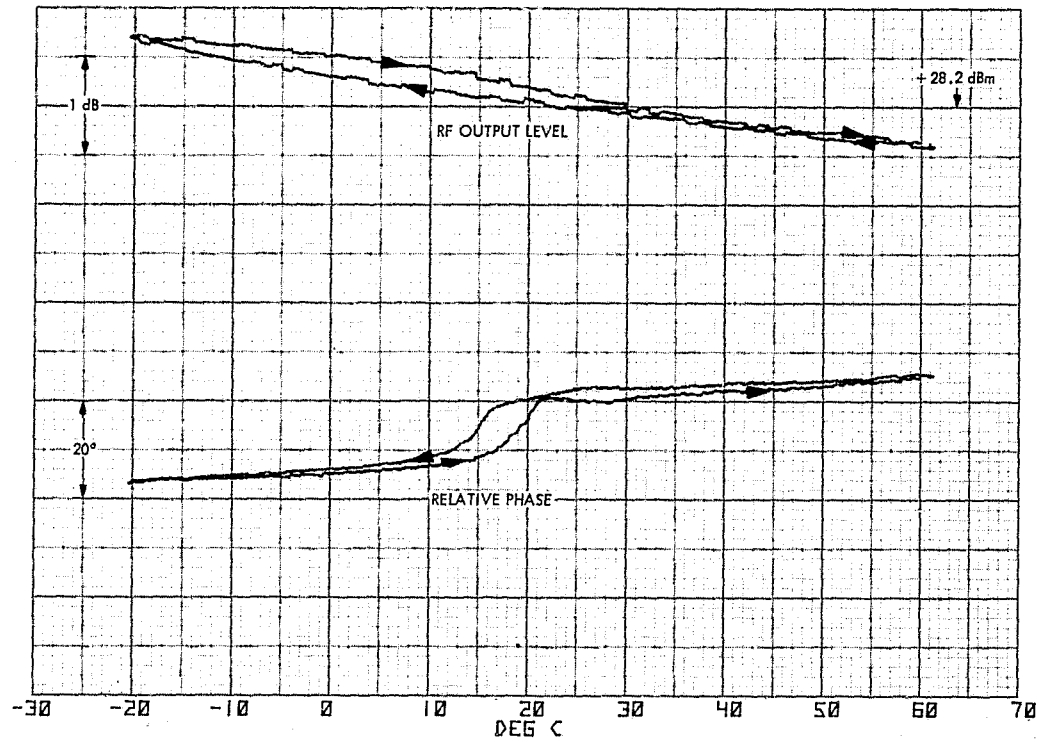

Figure 2-3. Phase and Amplitude Versus Temperature at f_o for Real-Time Raw Data (S/N 23)

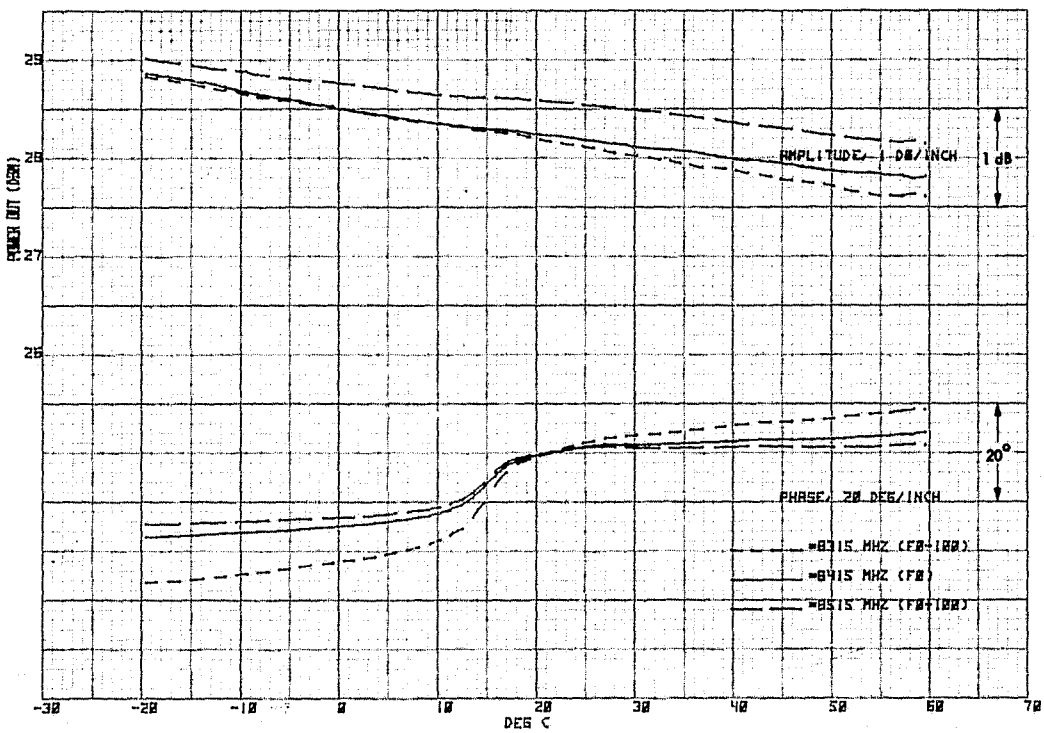

Figure 2-4. Phase and Amplitude Versus Temperature for Data Reduced Format (S/N 23)

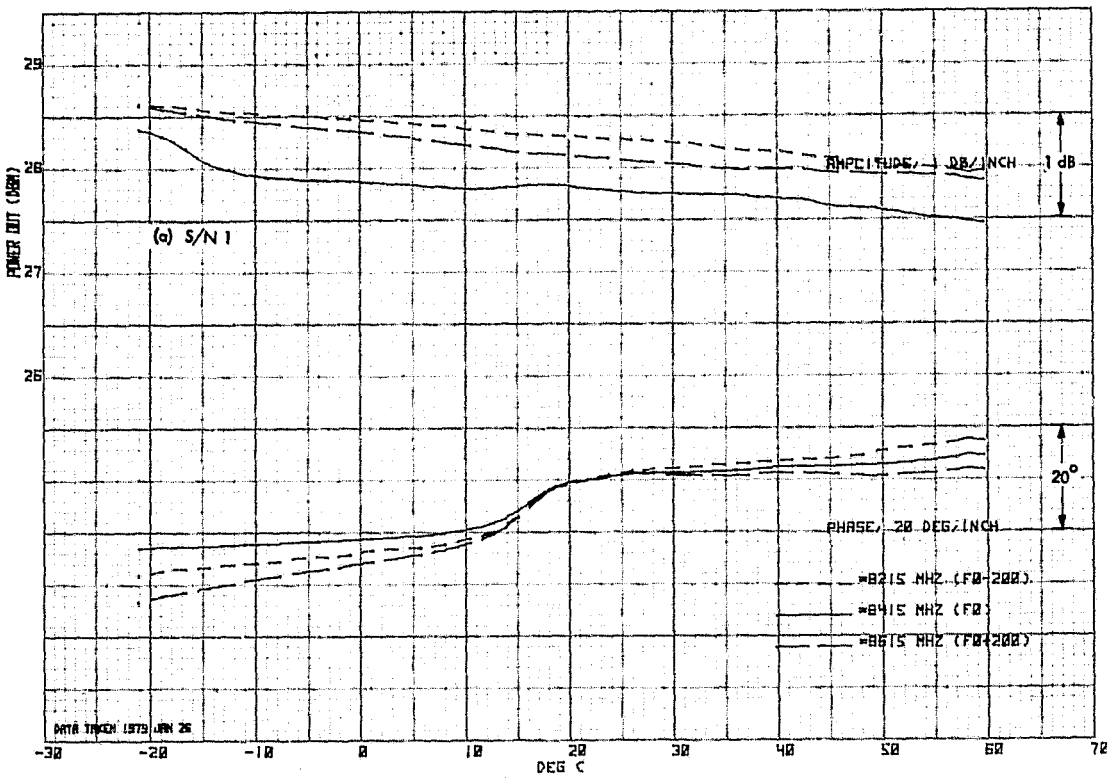

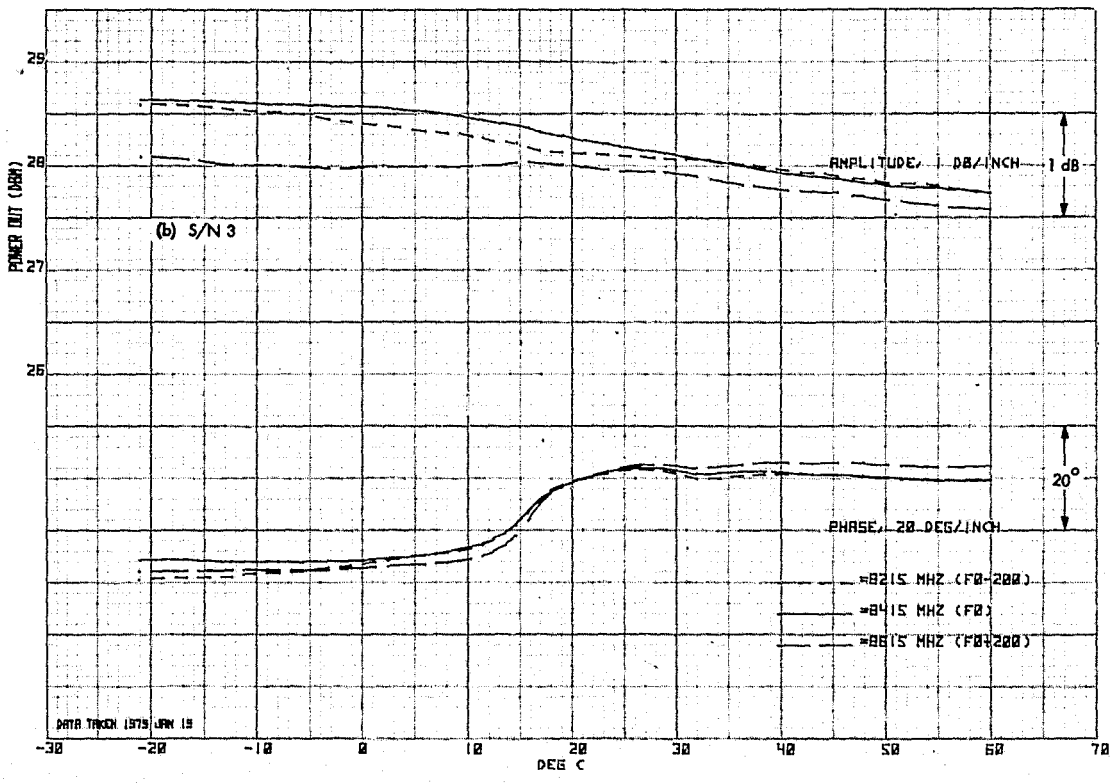

Figure 2-5. Phase and Amplitude Versus Temperature for 10 Modules

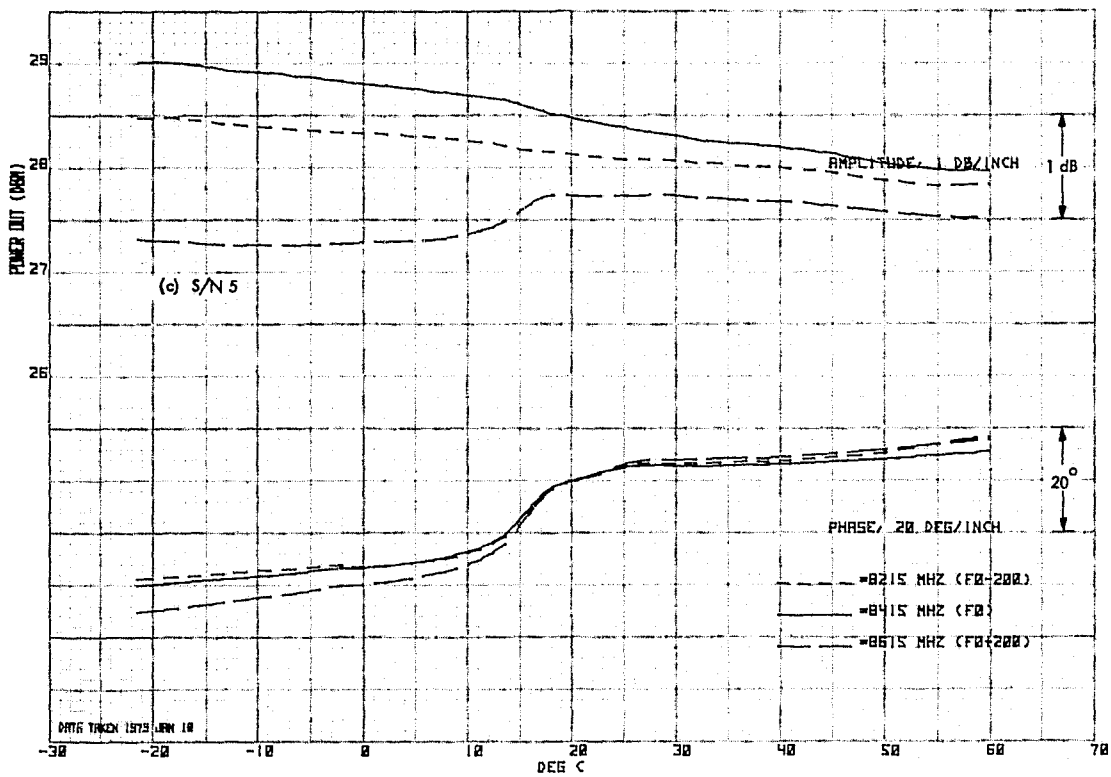

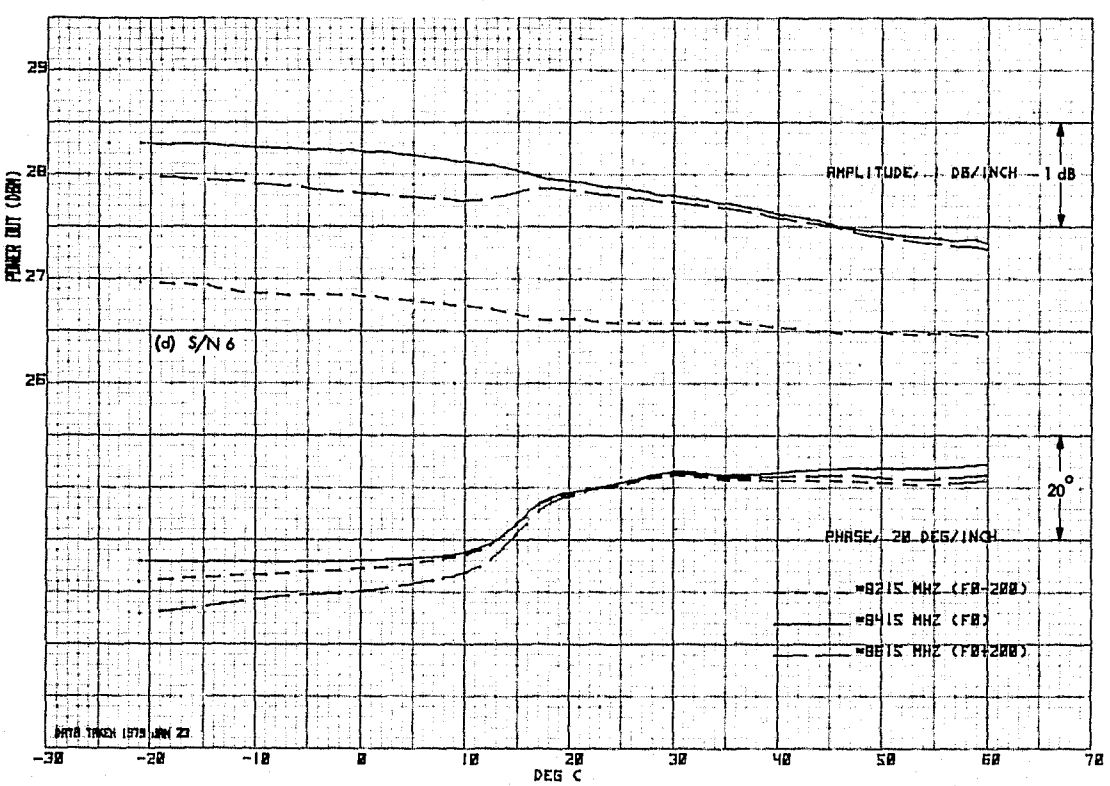

Figure 2-5. Phase and Amplitude Versus Temperature for 10 Modules (Continuation 1)

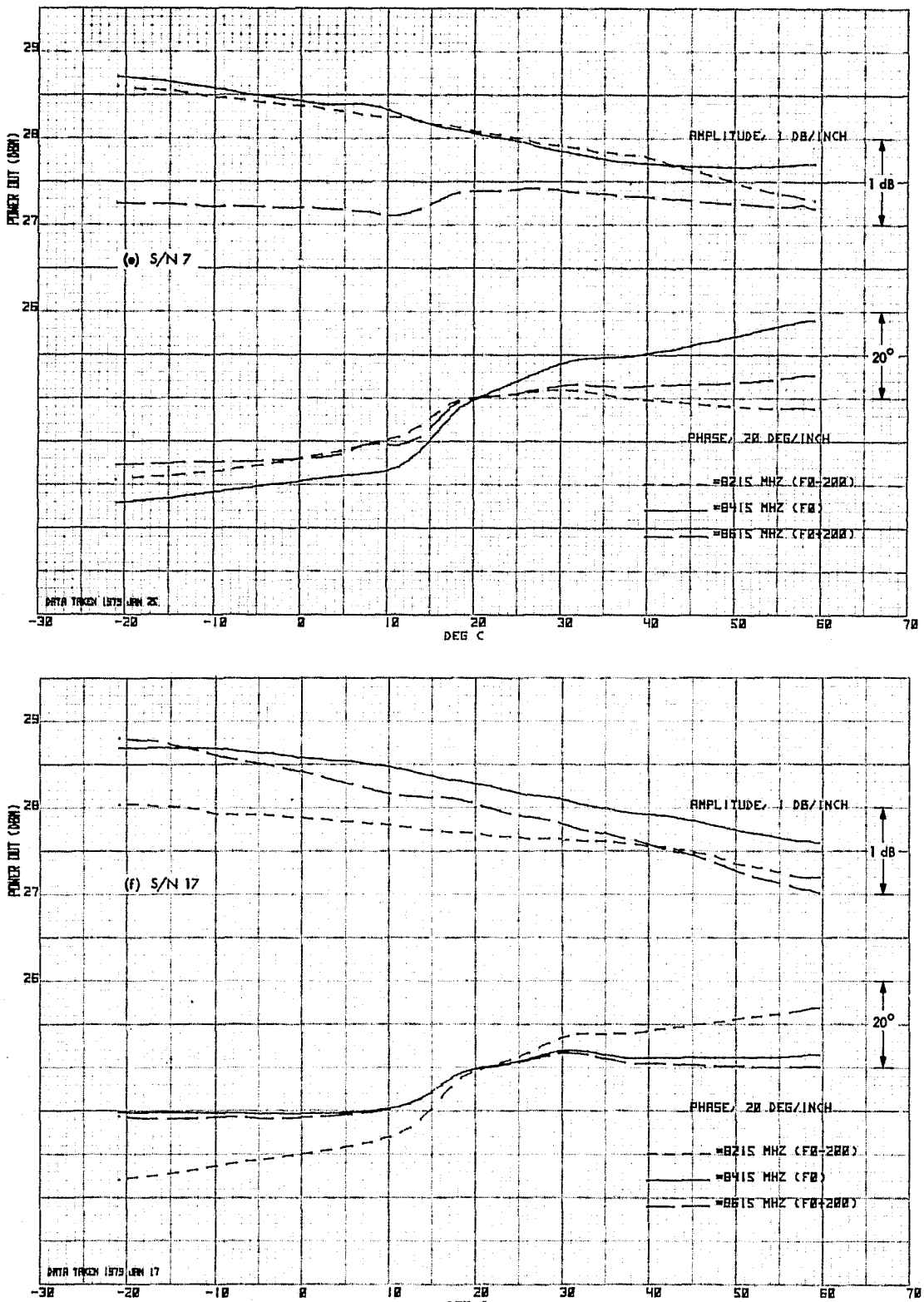

Figure 2-3. Phase and Amplitude Versus Temperature for 10 Modules (Continuation 2)

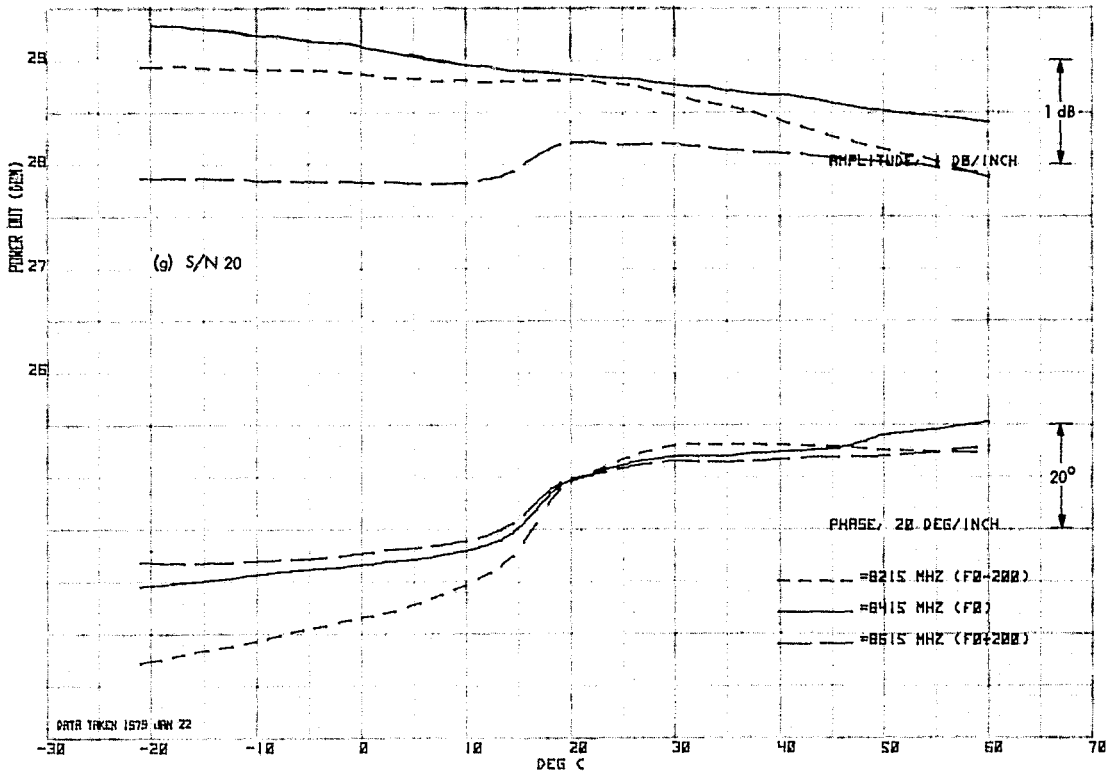

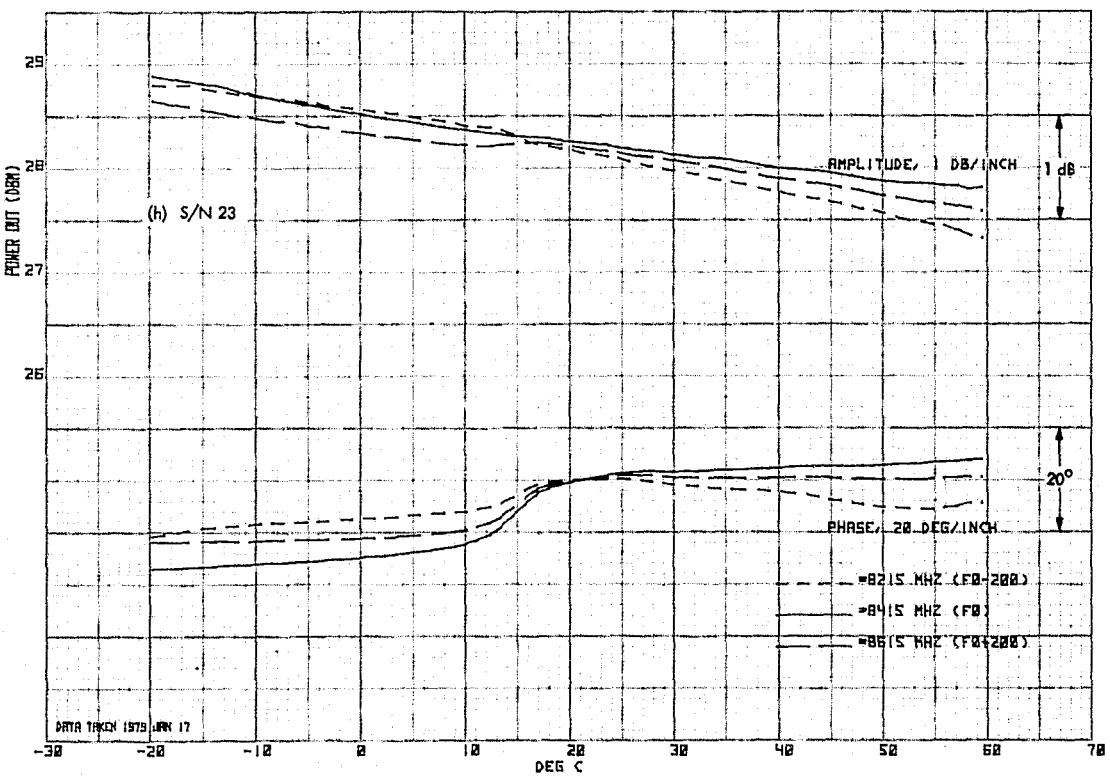

Figure 2-5. Phase and Amplitude Versus Temperature for 10 Modules (Continuation 3)

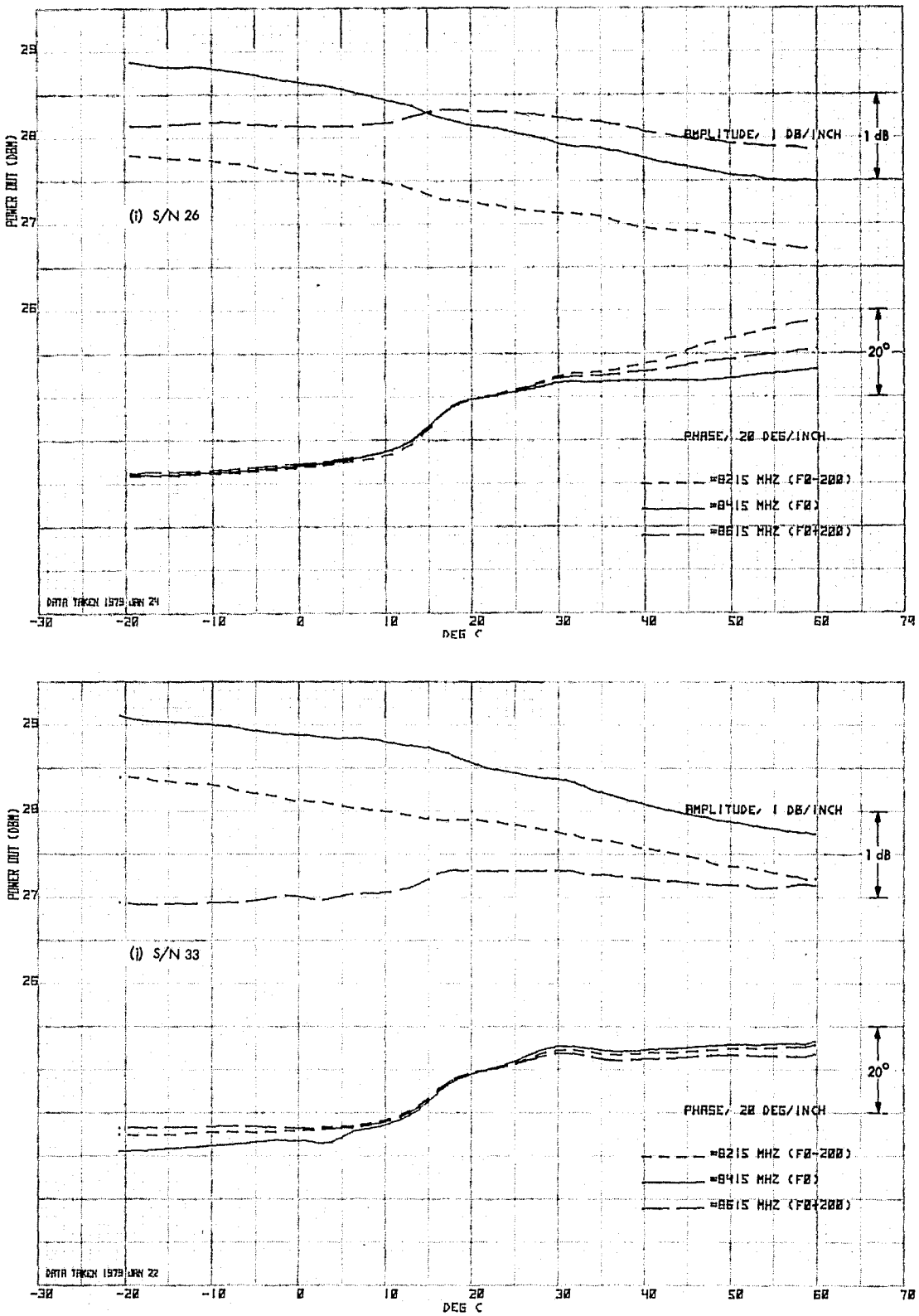

Figure 2-5. Phase and Amplitude Versus Temperature for 10 Modules (Continuation 4)

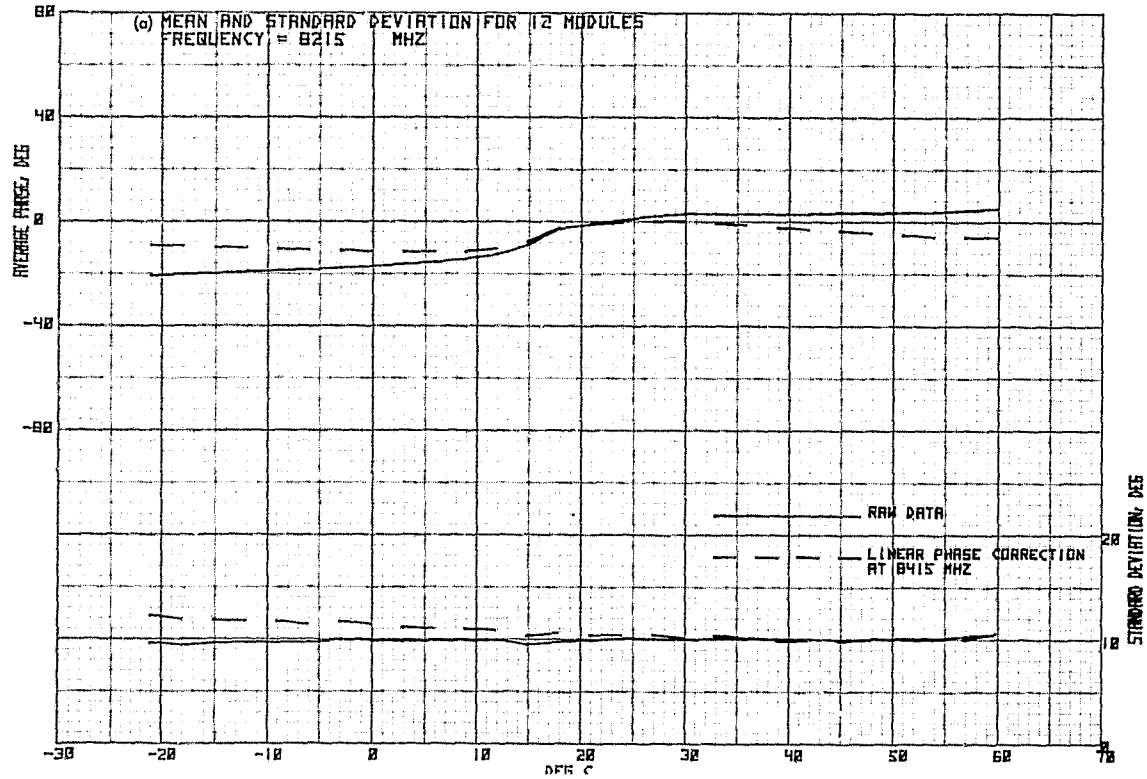

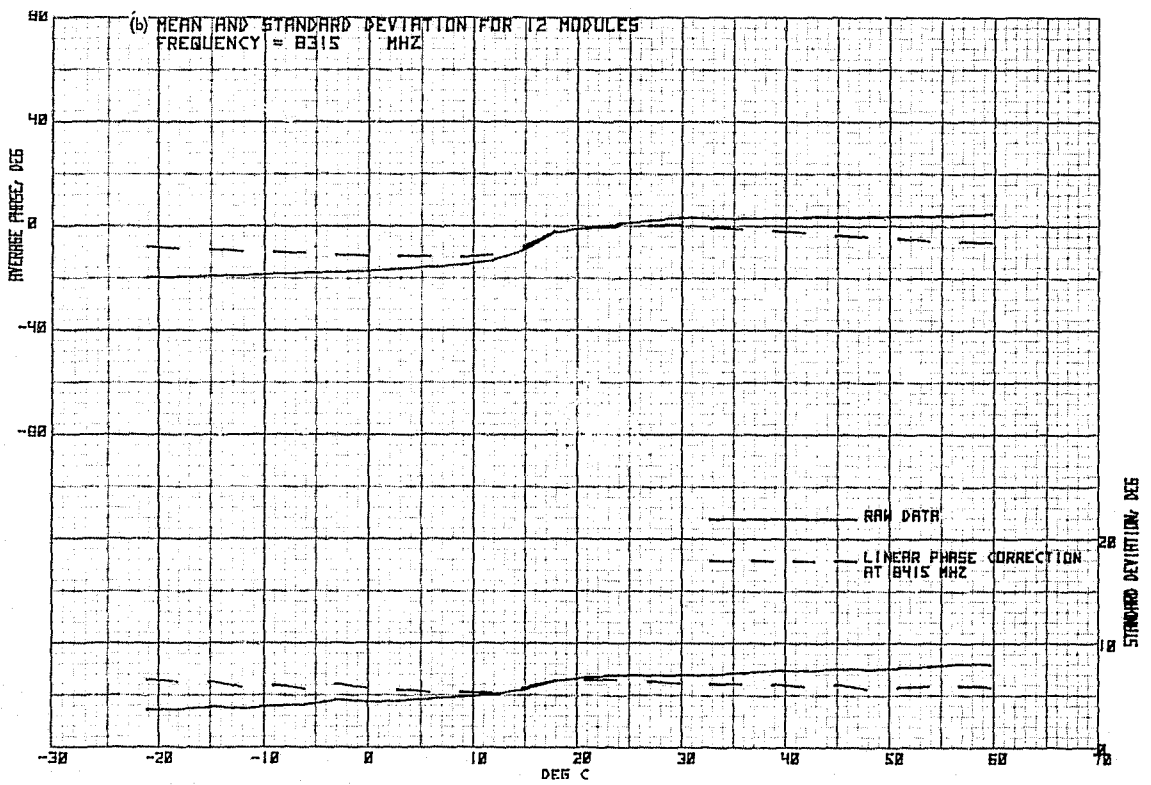

Figure 2-6. Amplifier Phase Statistics at Five Test Frequencies

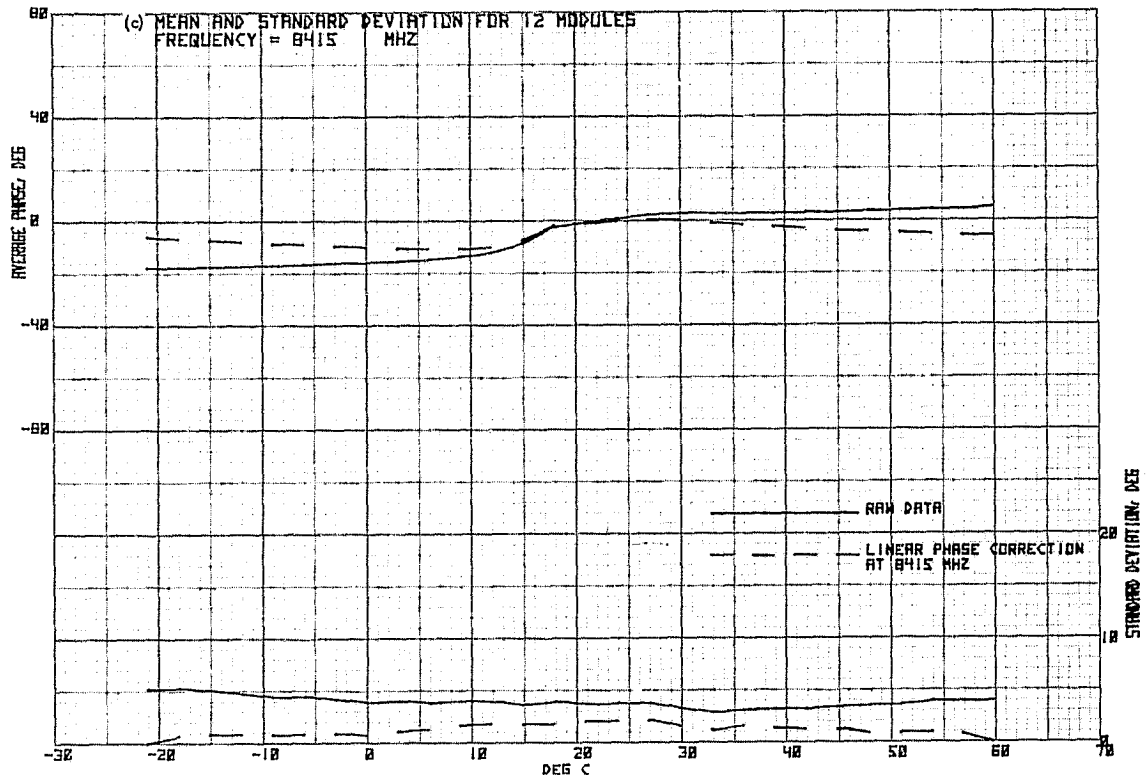

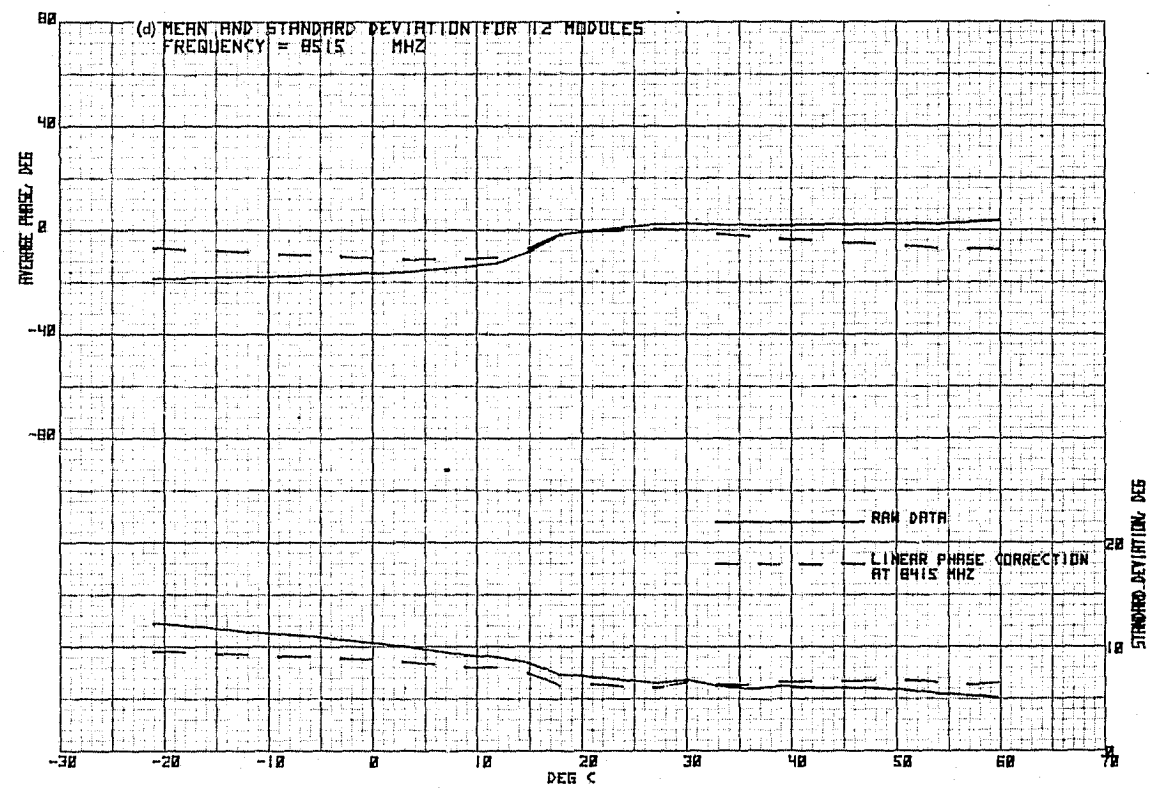

Figure 2-6. Amplifier Phase Statistics at Five Test Frequencies (Continuation 1)

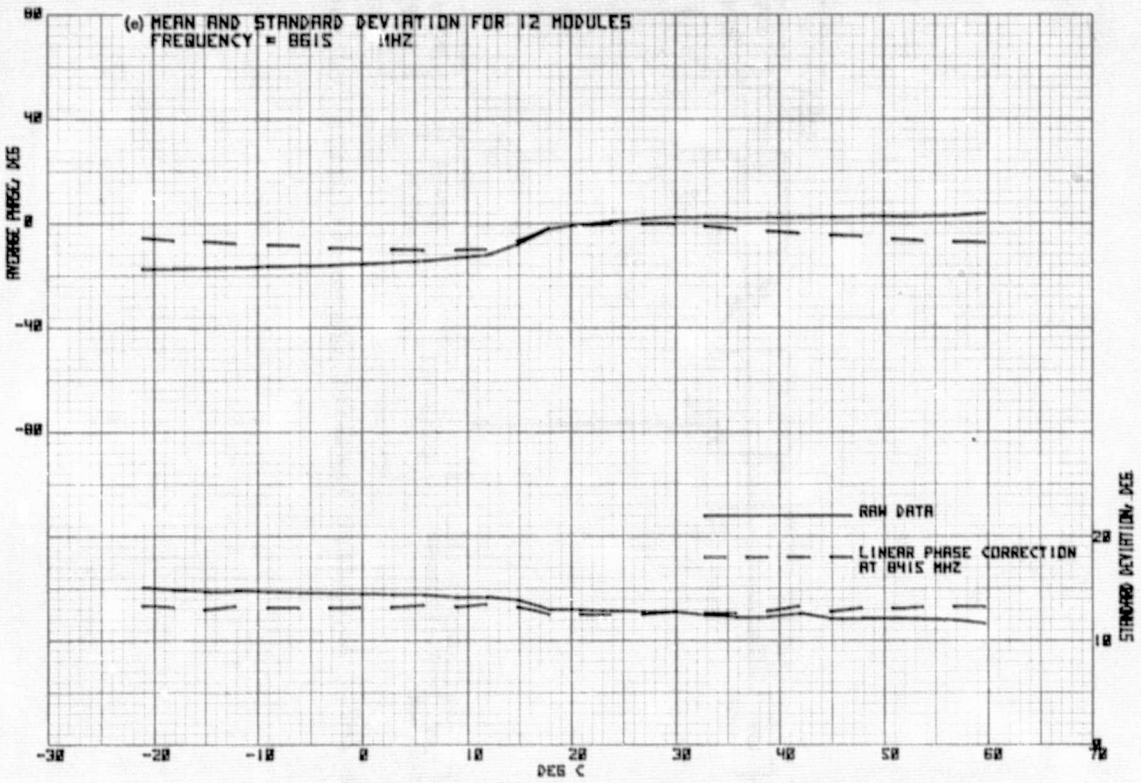

Figure 2-6. Amplifier Phase Statistics at Five Test Frequencies (Continuation 2)

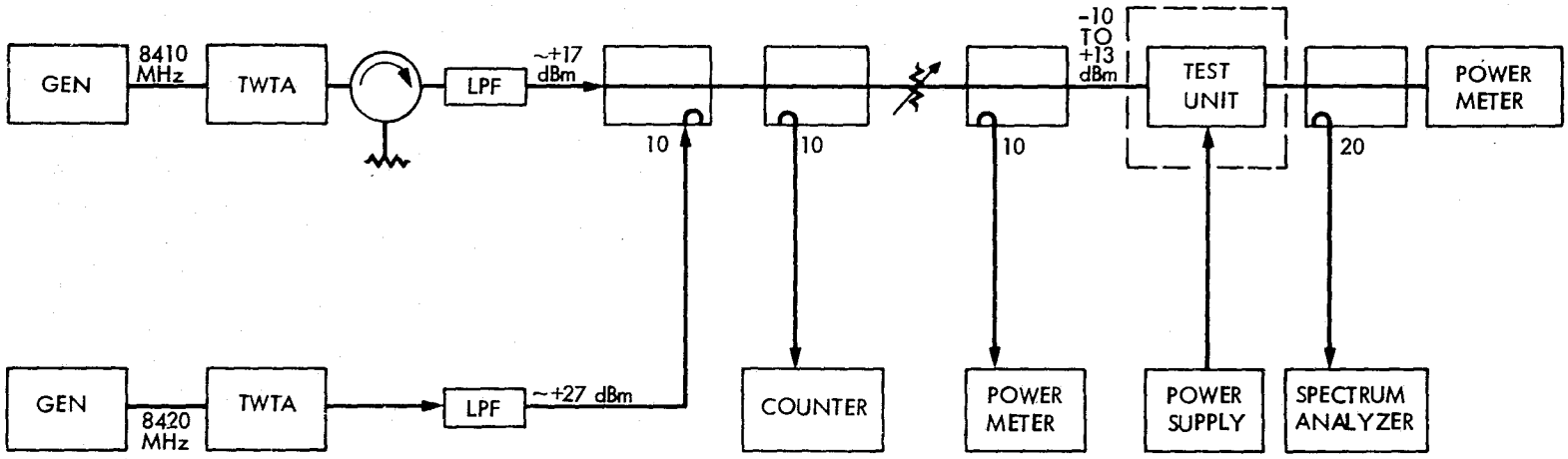

Figure 2-7. Amplifier Transfer Characteristics Test Set

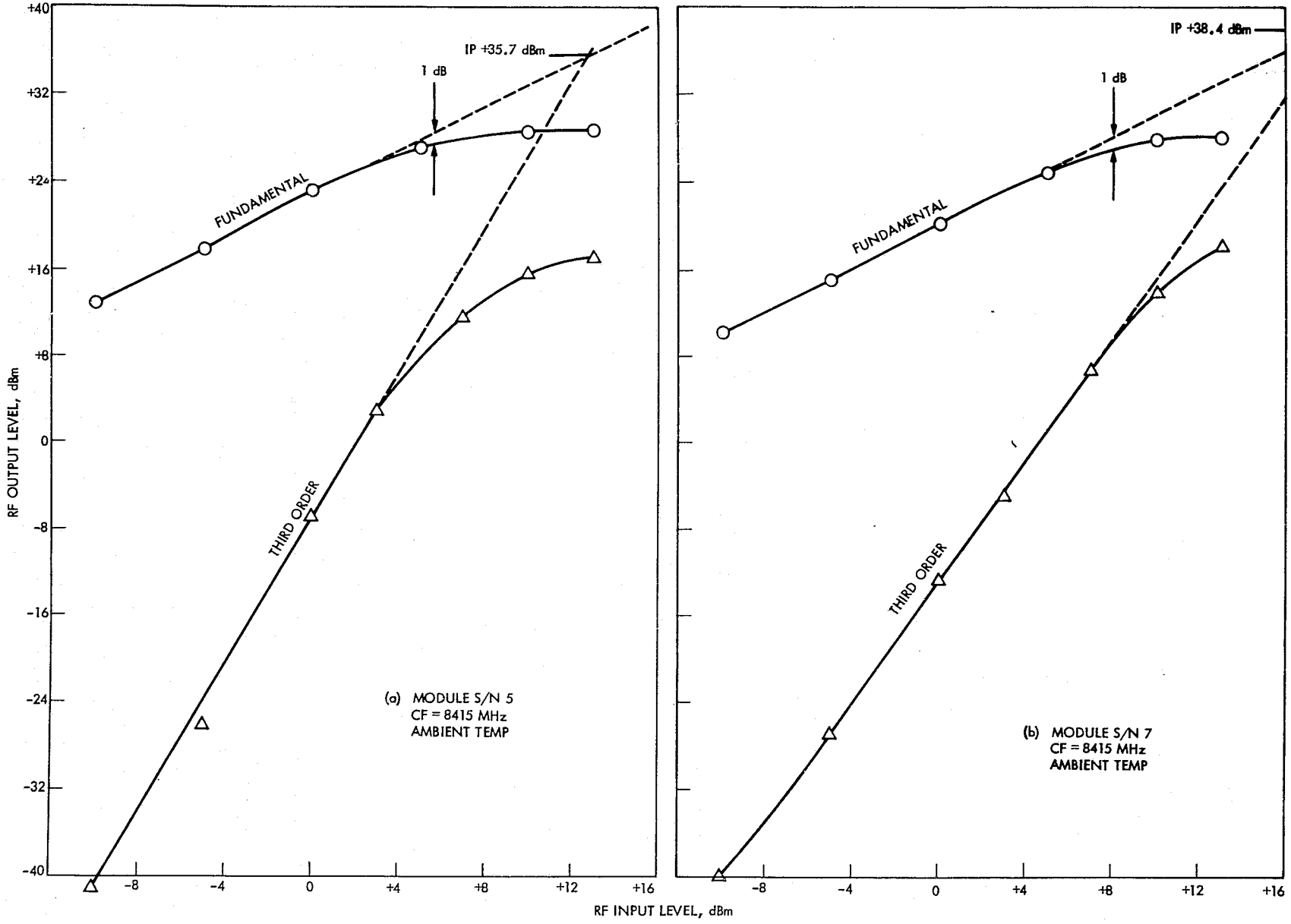

Figure 2-8. Amplifier Transfer Characteristics for Six Modules

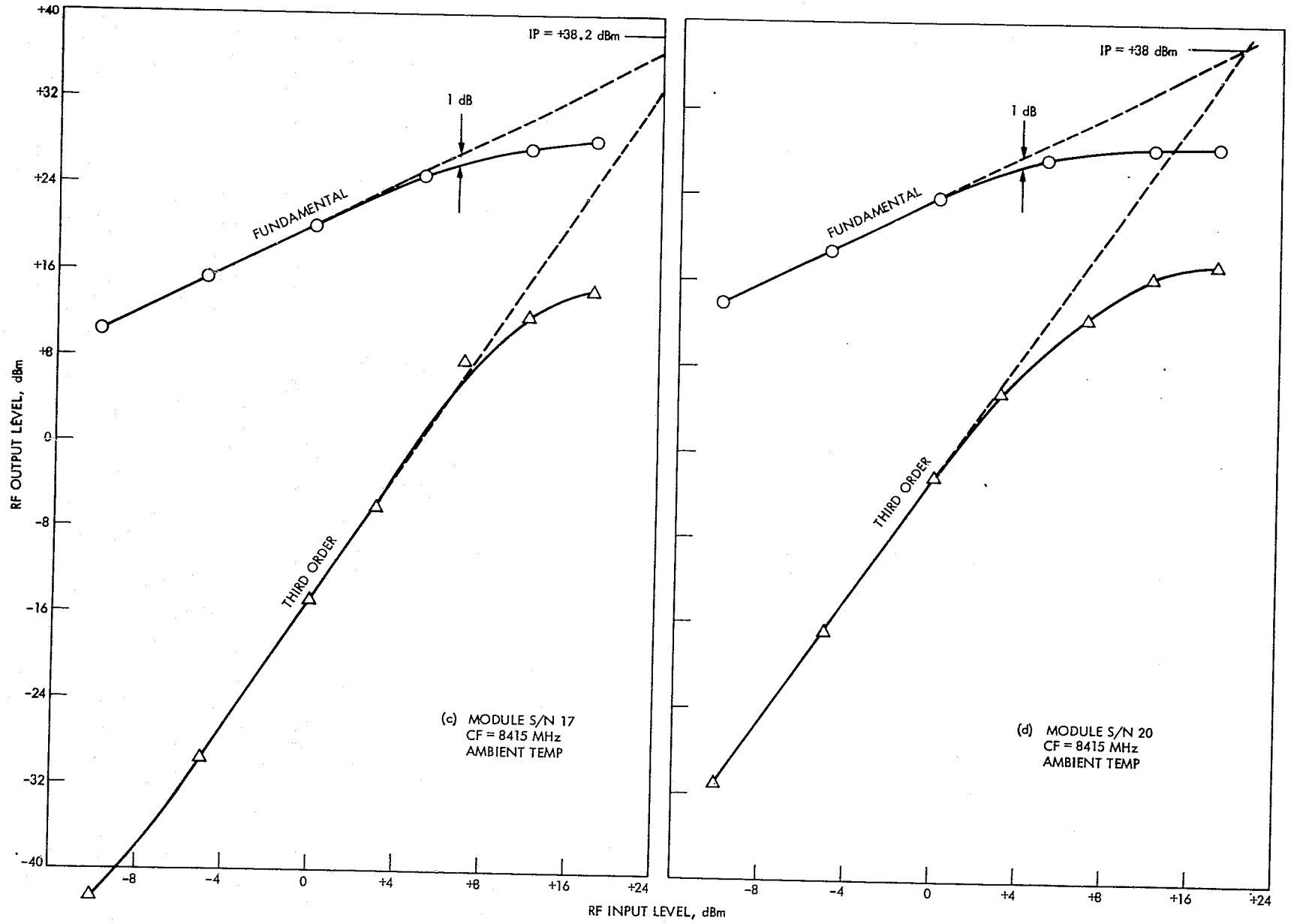

Figure 2-8. Amplifier Transfer Characteristics for Six Modules (Continuation 1)

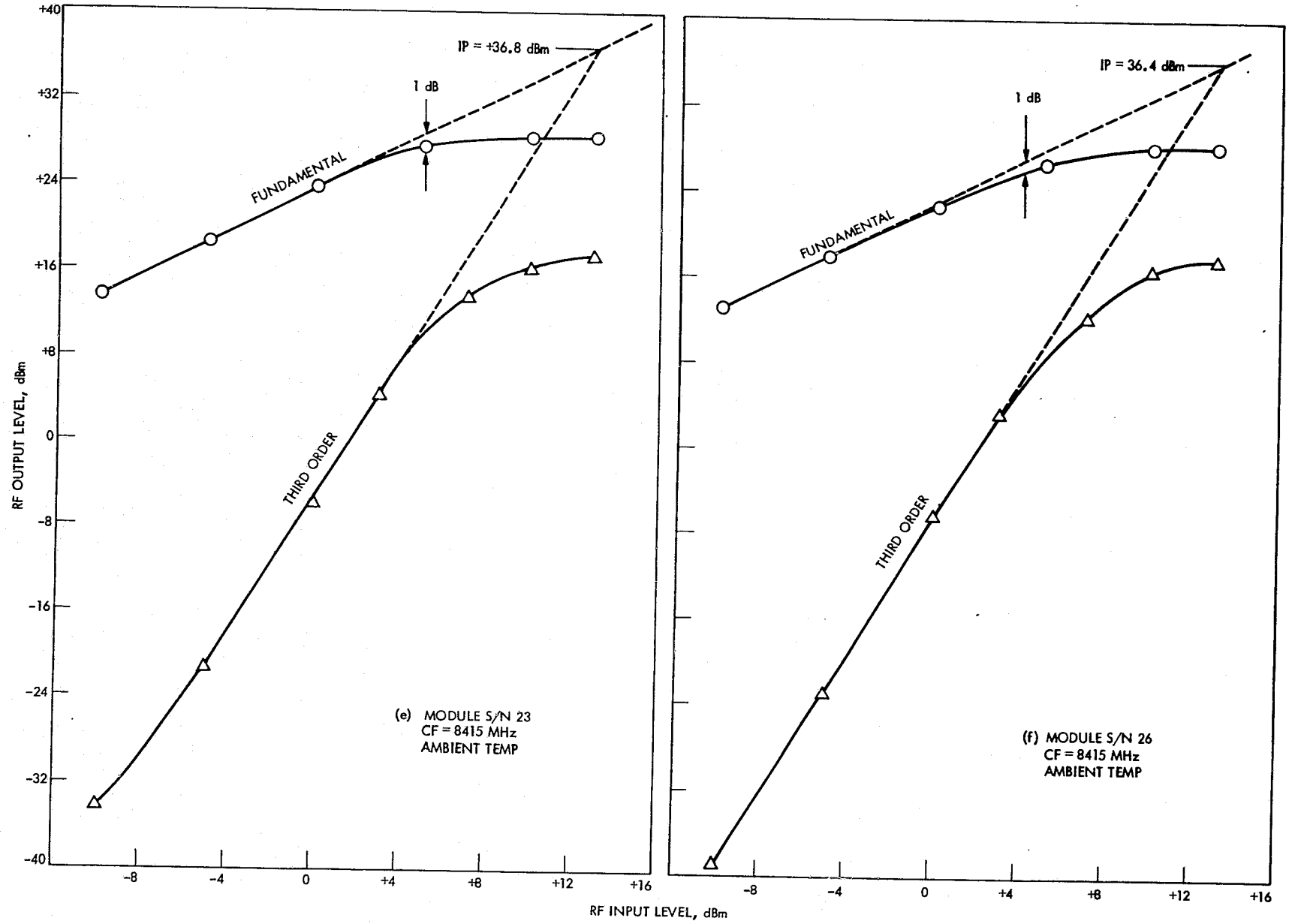

Figure 2-8. Amplifier Transfer Characteristics for Six Modules (Continuation 2)

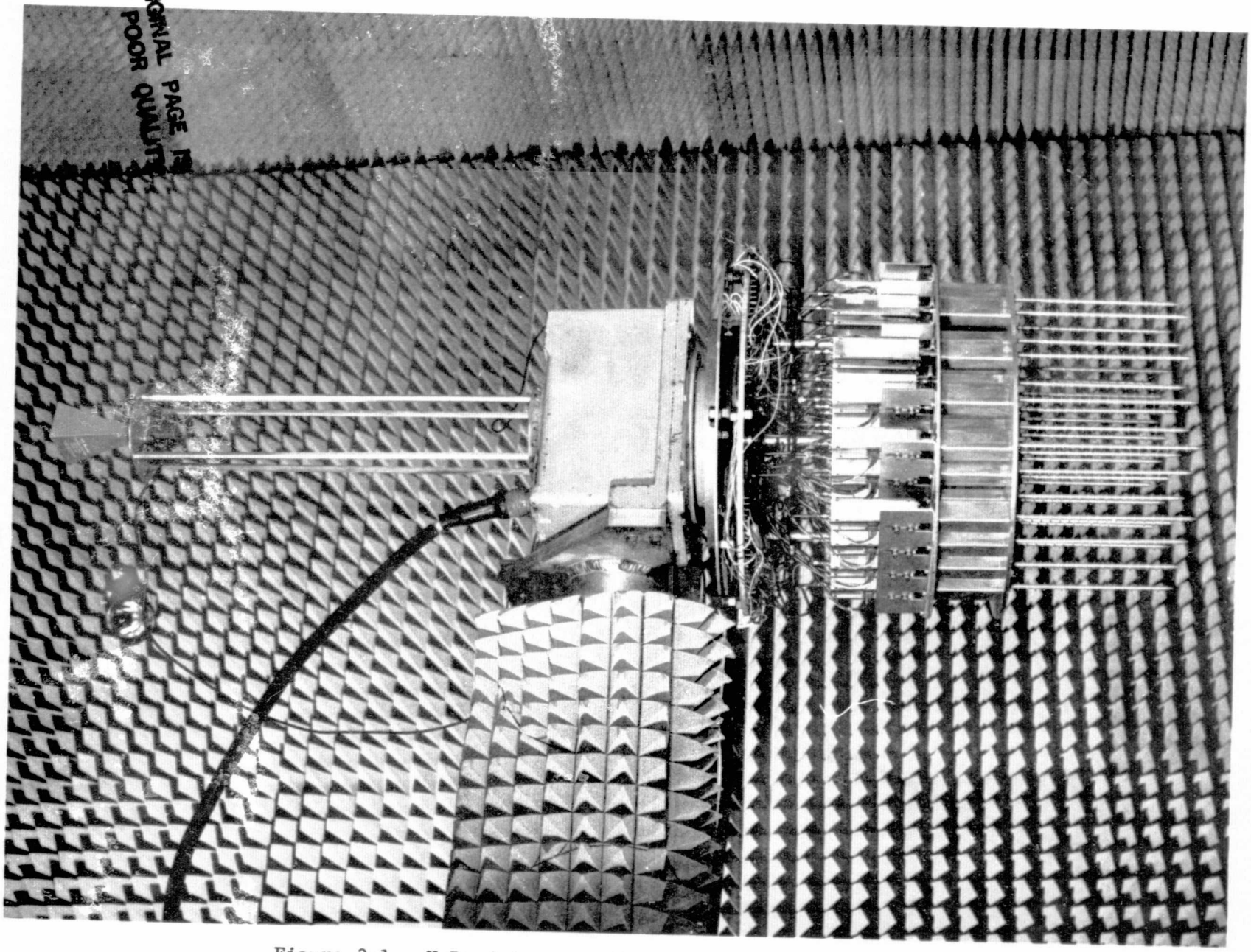

Figure 3-1. X-Band Array on Positioner in Anechoic Chamber

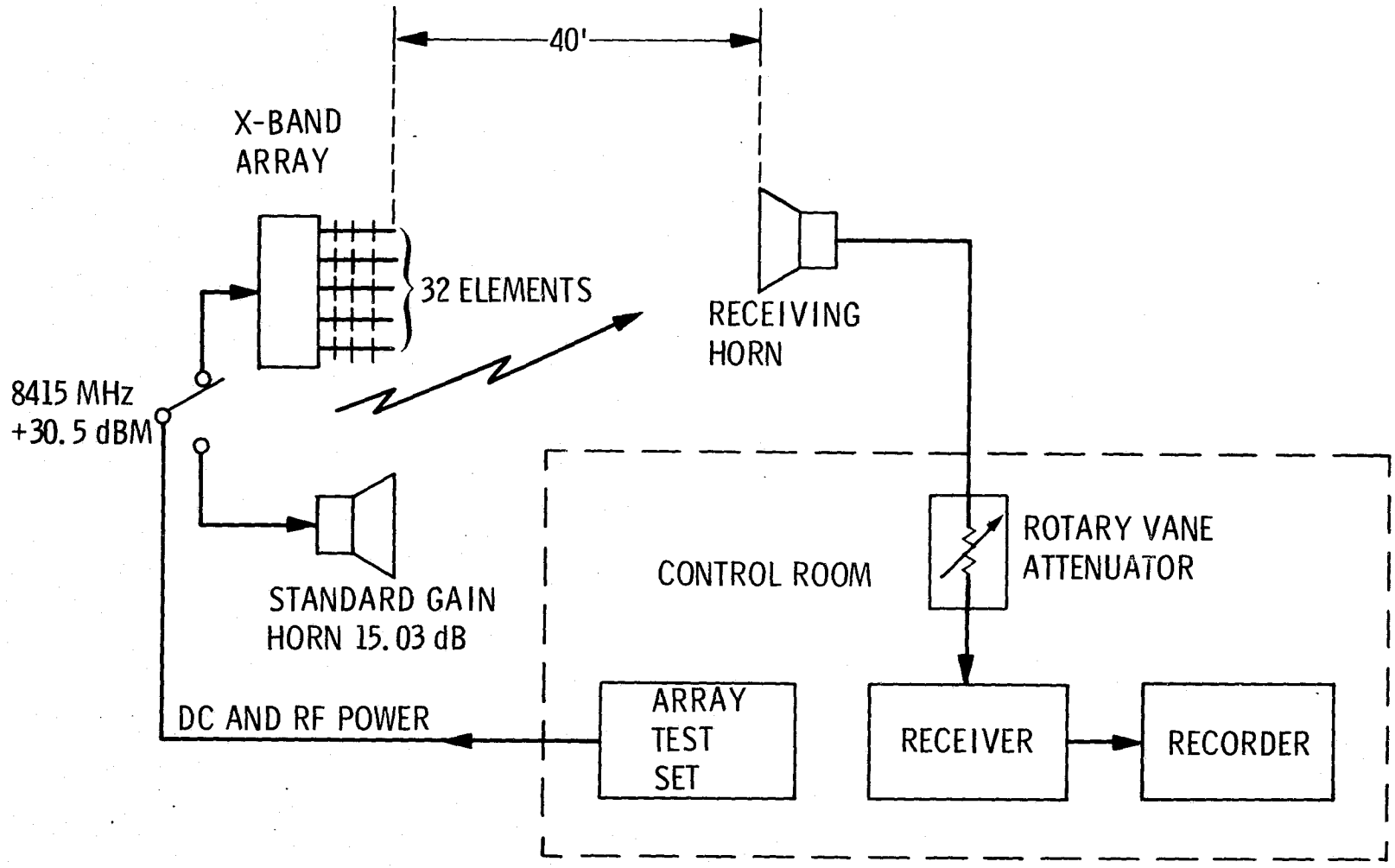

Figure 3-2. Antenna Range Measurement System Block Diagram

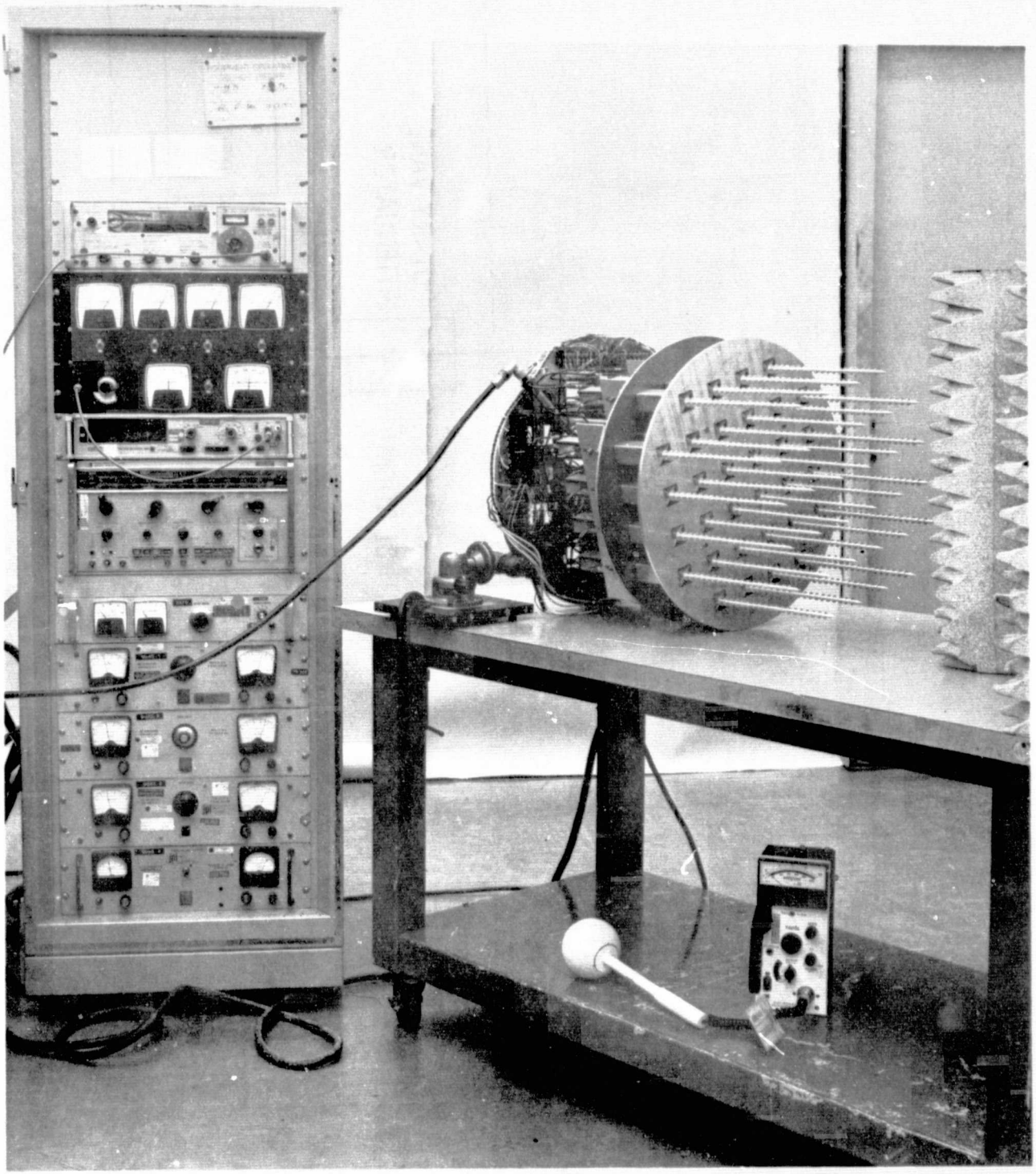

Figure 3-3. 32-Element Array and Test Set

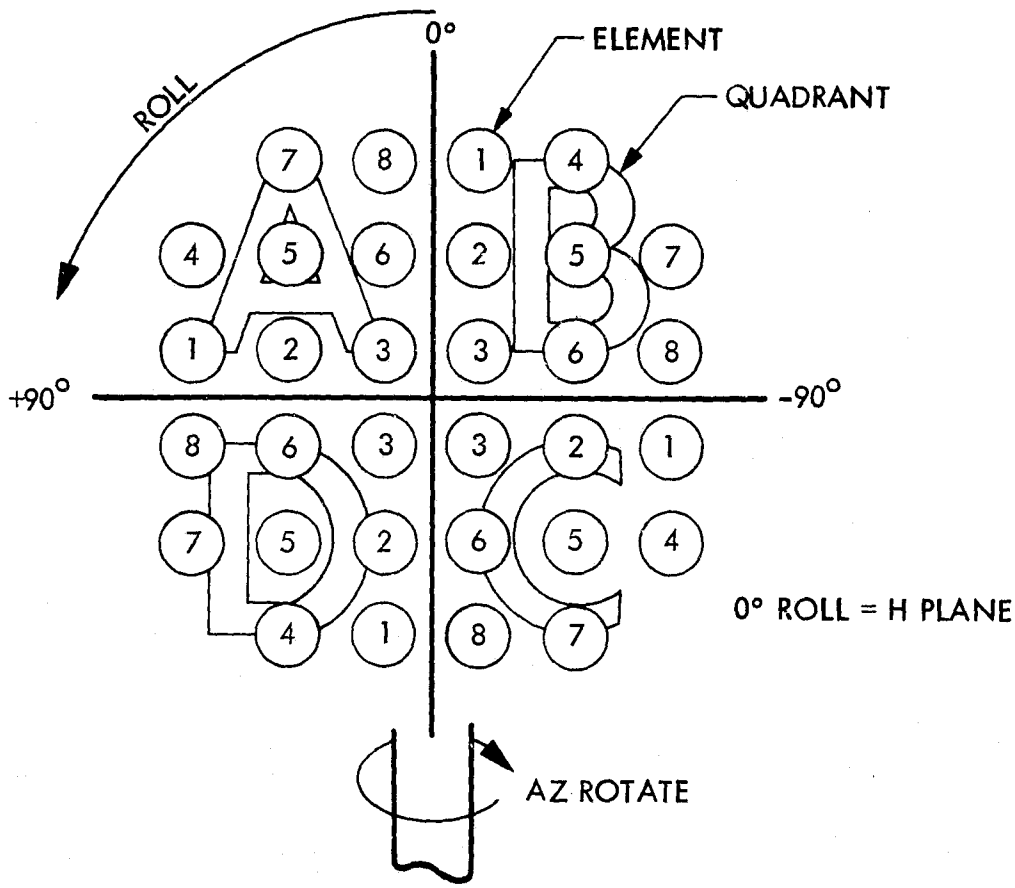

Figure 3-4. Array Element Configuration

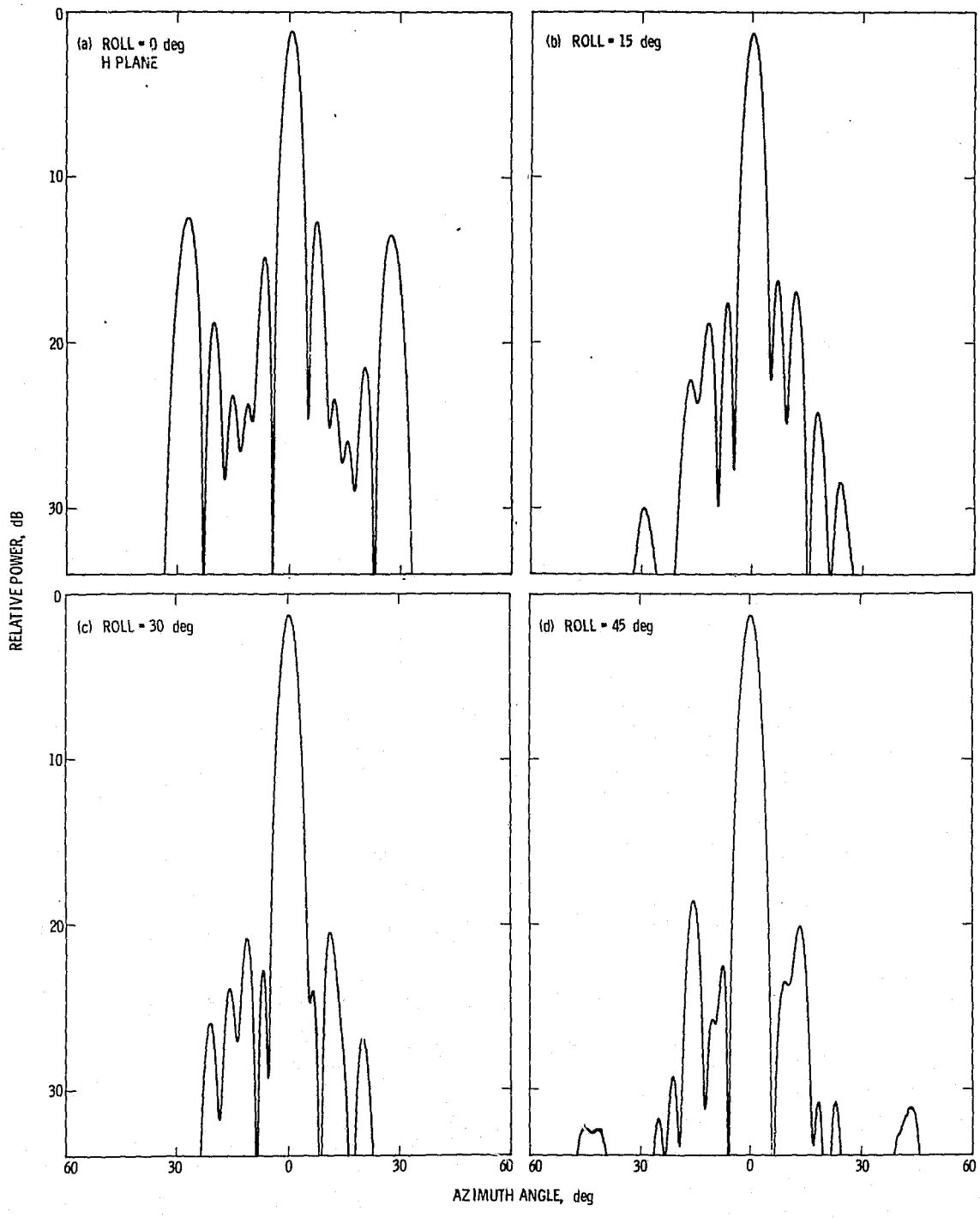

Figure 3-5. Array Standard Pattern Set

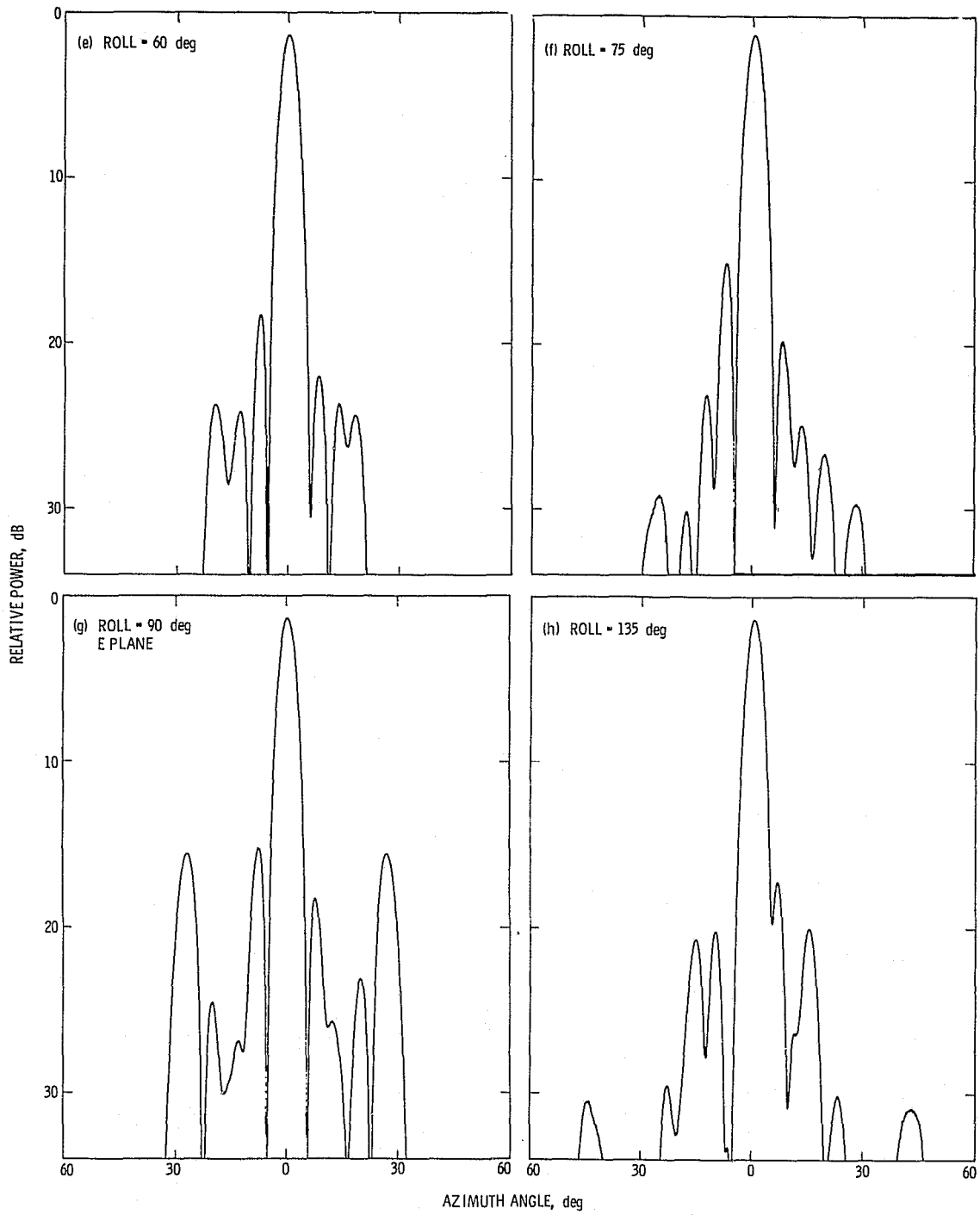

Figure 3-5. Array Standard Pattern Set (Continuation 1)

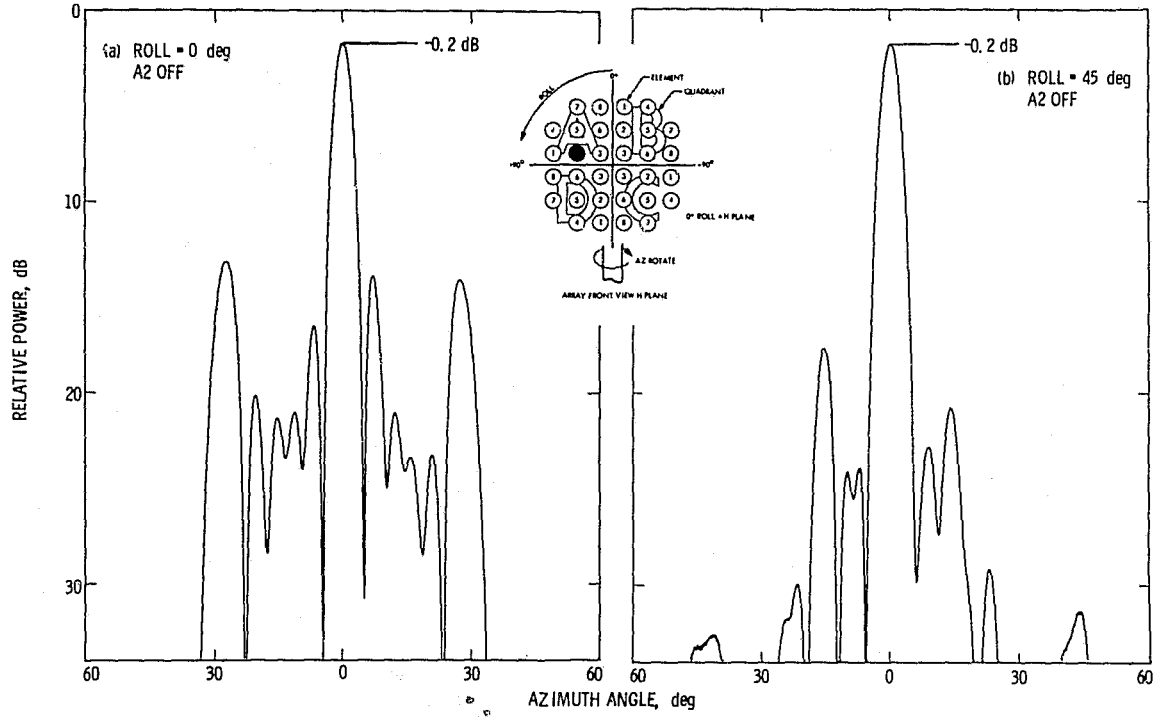

Figure 3-6. Array Patterns With One Module Unpowered

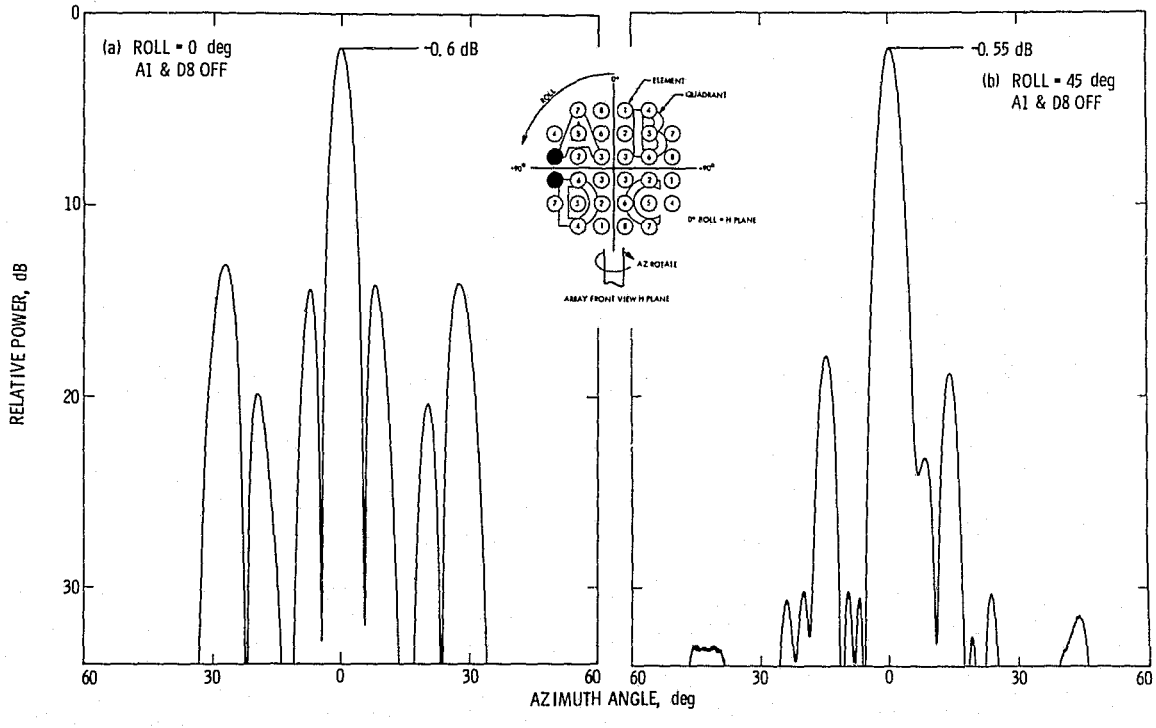

Figure 3-7. Array Patterns With Two Modules Unpowered

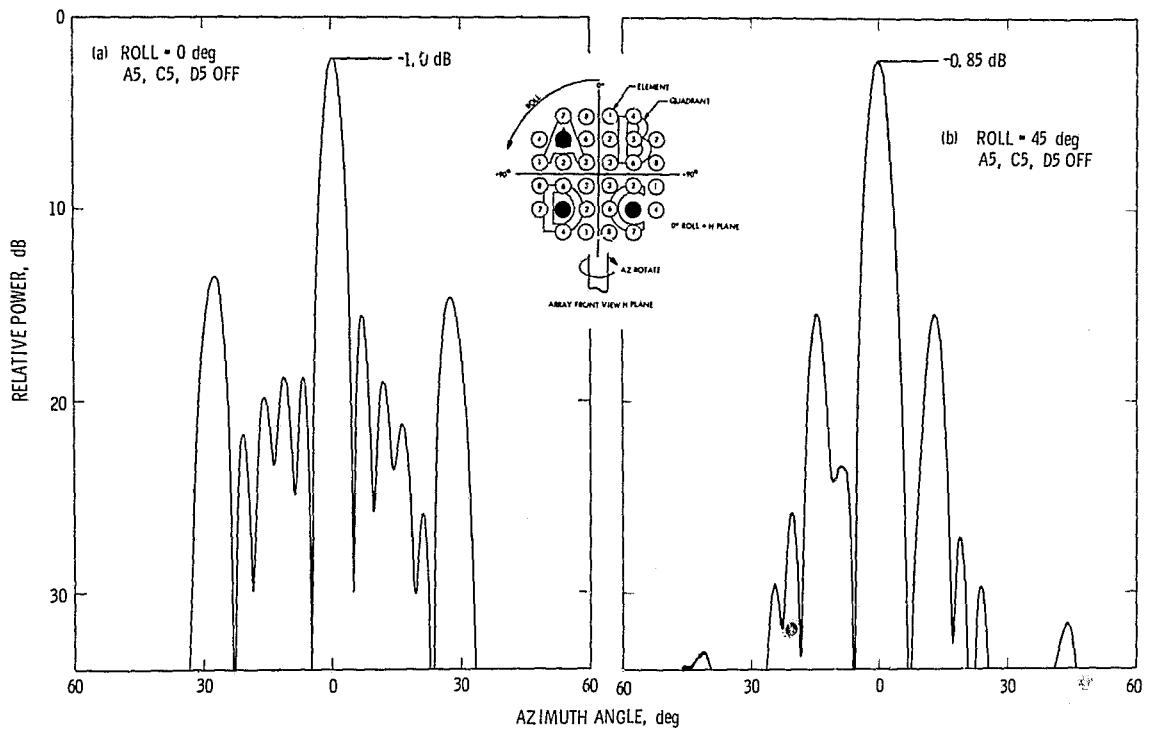

Figure 3-8. Array Patterns With Three Modules Unpowered

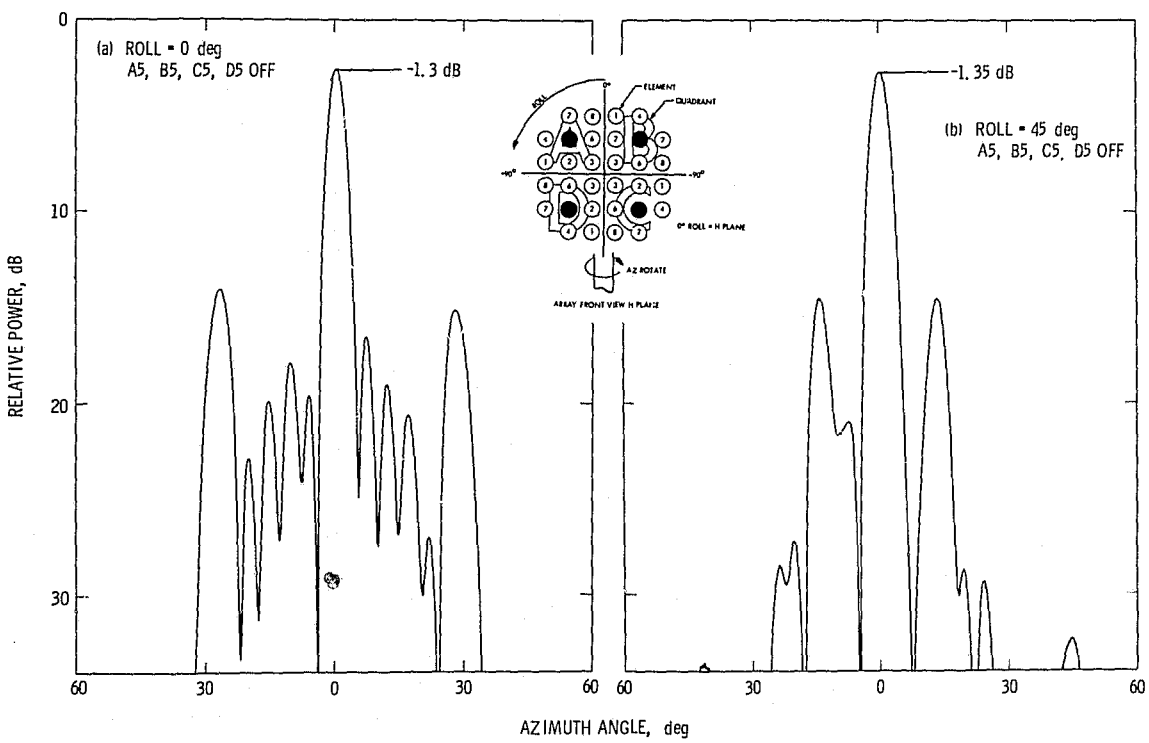

Figure 3-9. Array Patterns With Four Modules Unpowered

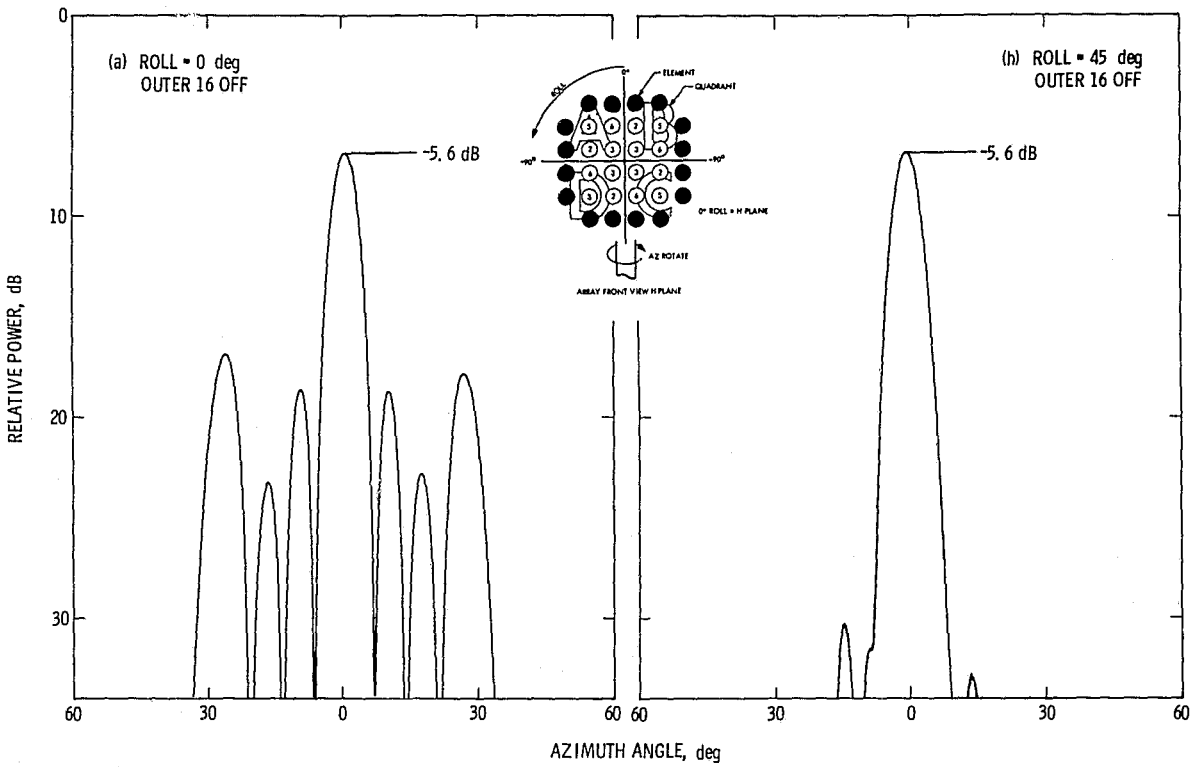

Figure 3-10. Array Patterns With Outer 16 Modules Unpowered

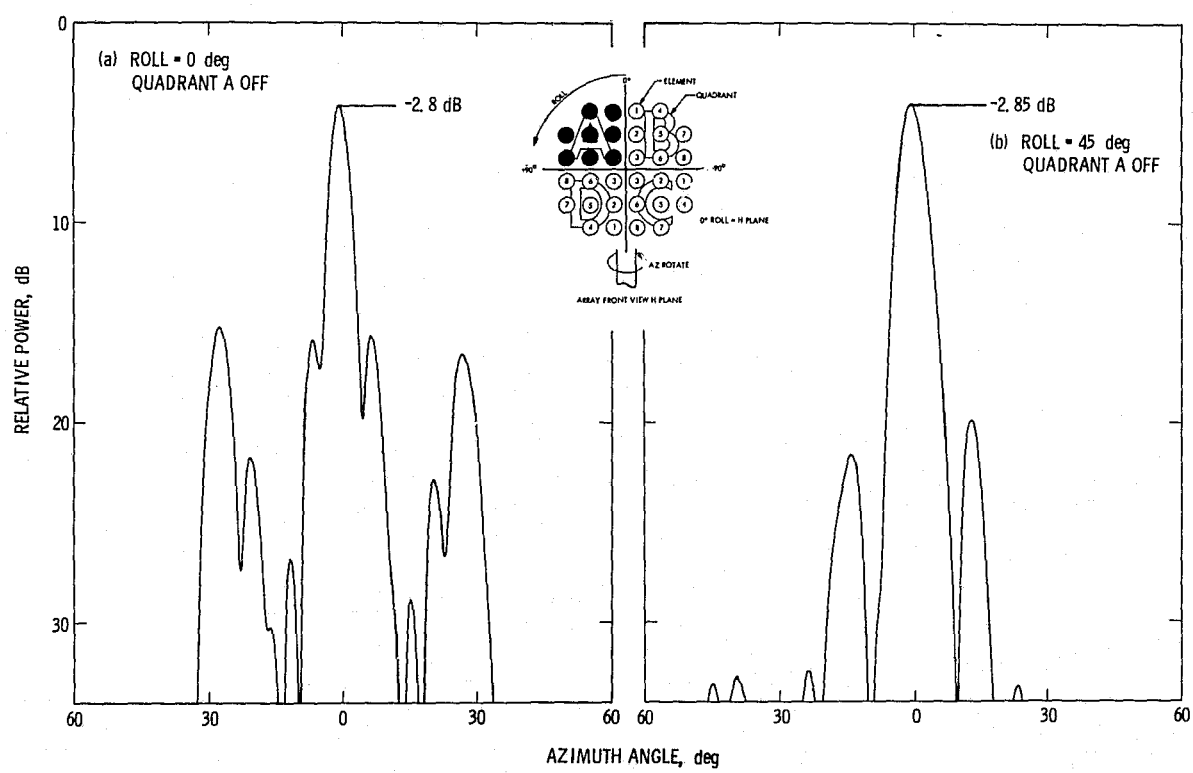

Figure 3-11. Array Patterns With One Quadrant Unpowered

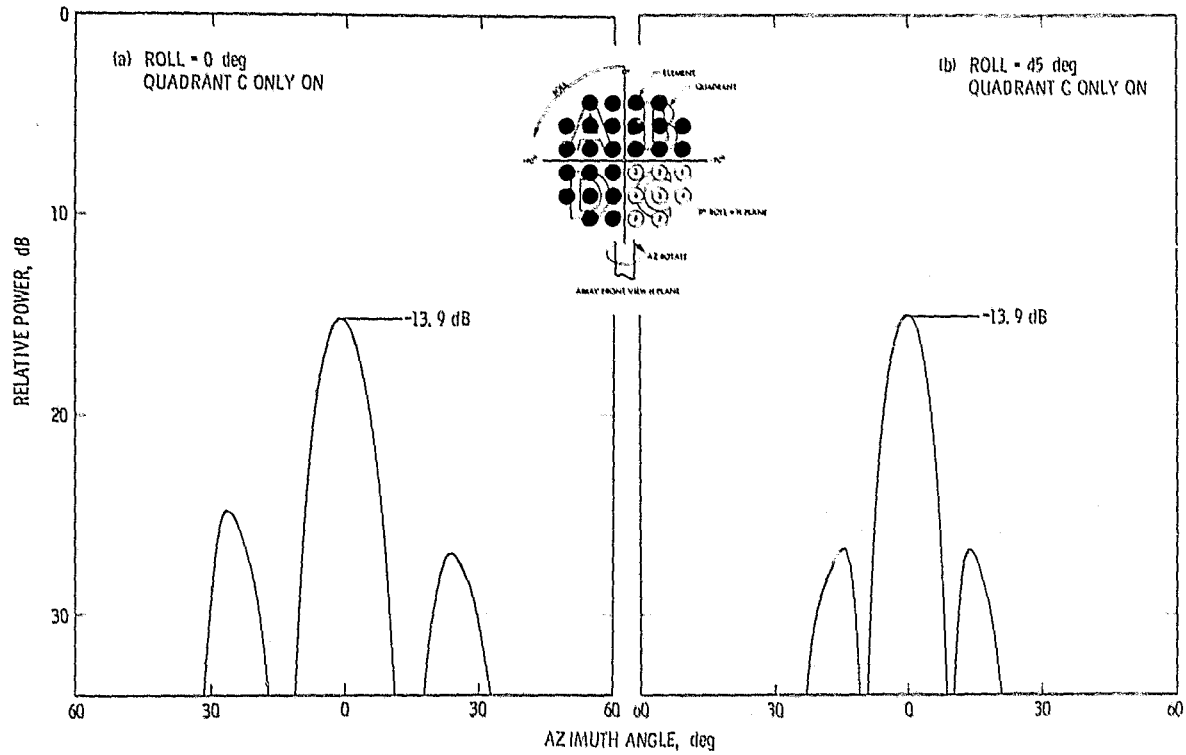

Figure 3-12. Array Patterns With Three Quadrants Unpowered

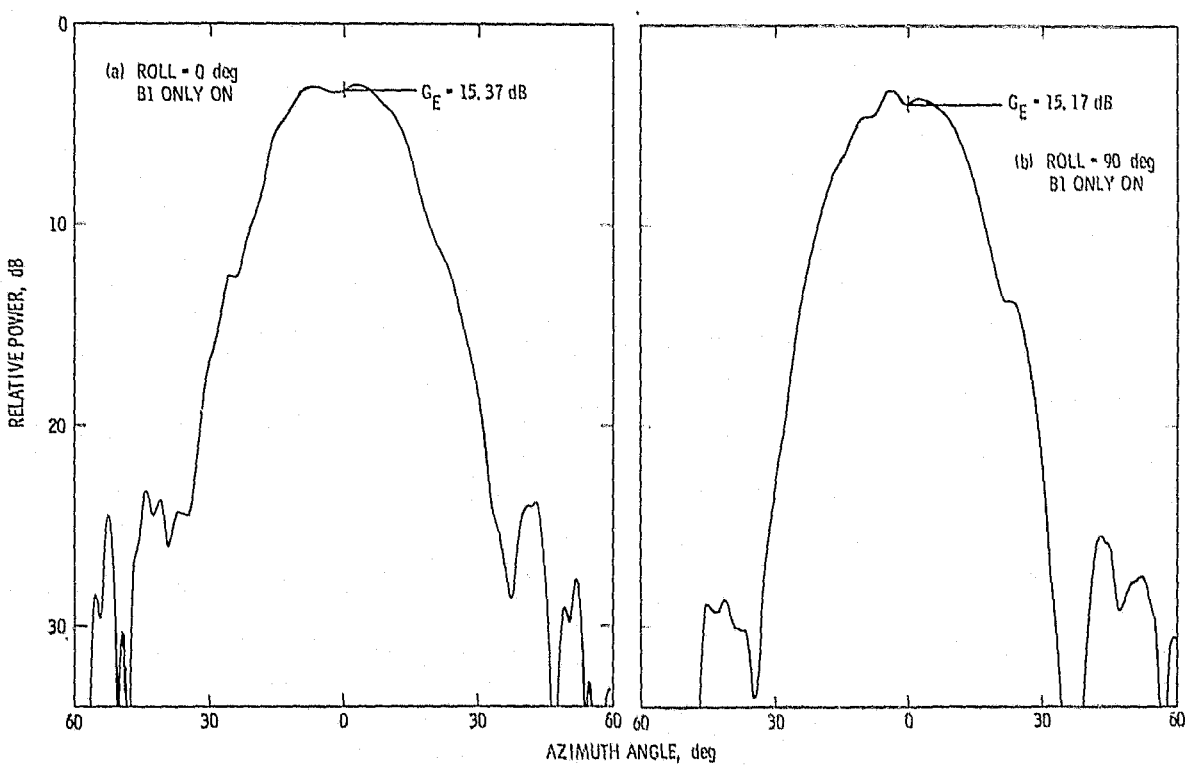

Figure 3-13. Single Element Patterns With 31 Modules Unpowered

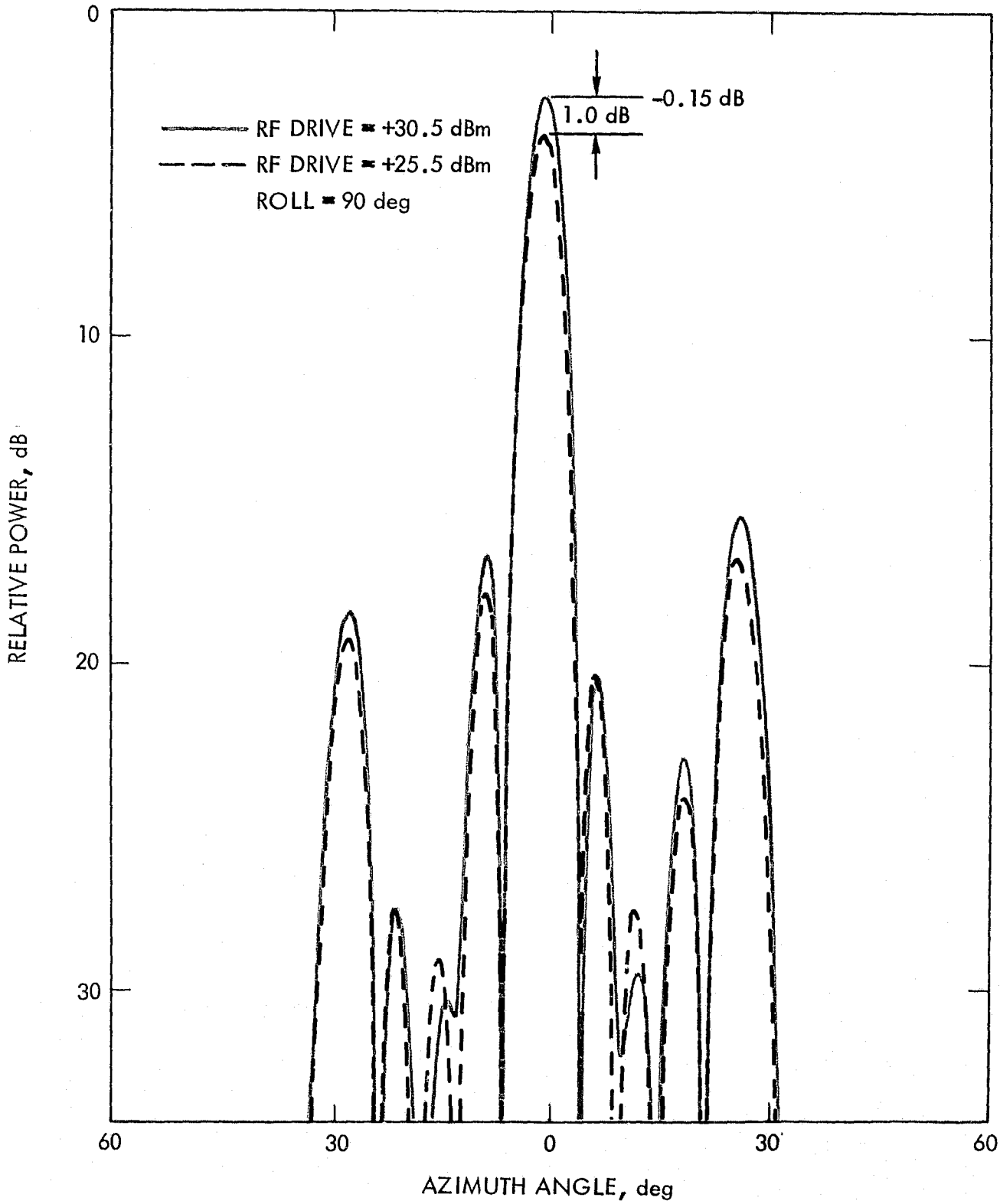

Figure 3-14. Array Beam Shifted Pattern With Input Drive Test

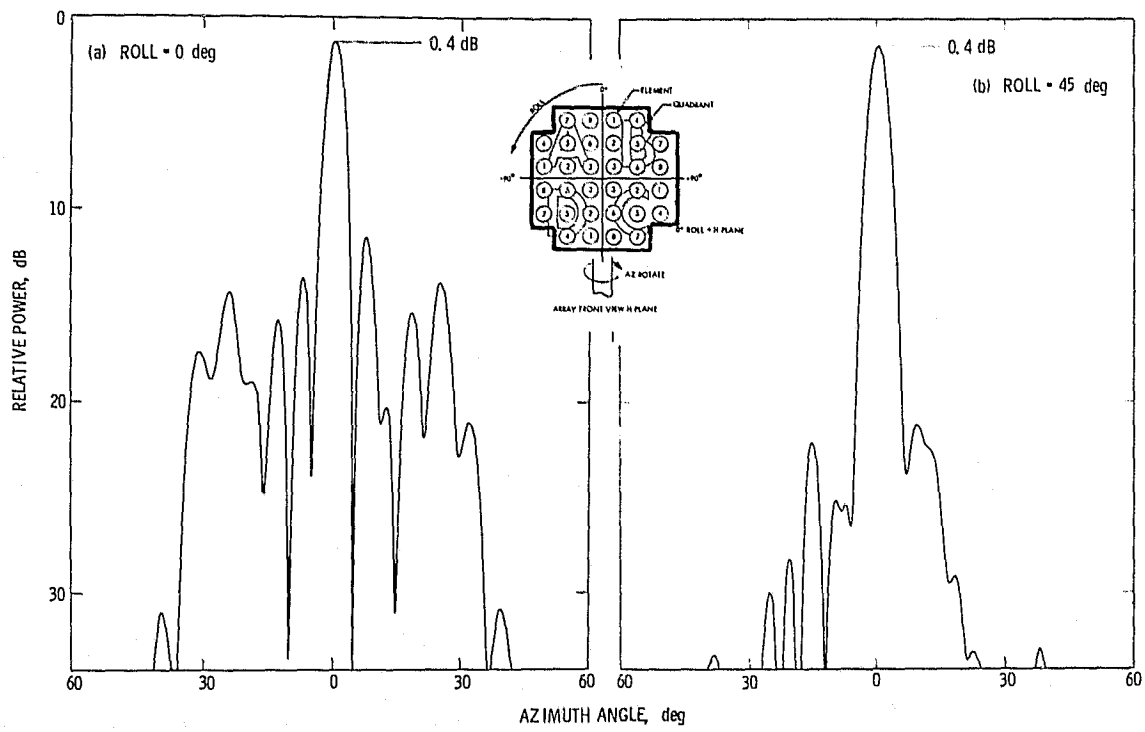

Figure 3-15. Shield Experiment Patterns

APPENDIX A

TASK ORDER REQUIREMENTS

FOR ACTIVE ARRAY EVALUATION

STATEMENT OF WORK

JPL shall support Headquarters SAMSO by conducting an evaluation of JPL's X-band 32 element active array. This effort includes the following tasks:

1. Perform antenna range measurements of the array of radiation patterns to ±30° off axis, peak gain, directivity of the array assembly in a normal operating mode as well as several degraded performance modes.

2. After disassembly of the array, each of 10 amplifier modules shall be evaluated for phase and amplitude stability over a frequency range 8.4 GHz ±200 MHz and versus temperature from -20°C to +50°C.

3. Based on the results of paragraph 2, compensation networks will be designed and integrated into each of the 10 amplifiers to stabilize the phase to less than ±10.0 degrees 1 sigma and the amplitude to ±1.0 dB (±0.5 dB as a goal) relative to their nominal output over the temperature range, and ±50 MHz centered at 8.415 GHz.

APPENDIX B

X-BAND HIGH-GAIN ANTENNA

WITH SOLID-STATE TRANSMITTER

X-BAND HIGH-GAIN ANTENNA WITH SOLID-STATE TRANSMITTER

K. Woo, J. Boreham, P. Cramer, R. Postal, B. Conroy,
R. Thomas, and W. Ackerknecht
Jet Propulsion Laboratory
California Institute of Technology
Pasadena, California 91103

A. 3.7-m X-band high gain spacecraft antenna fed with a "fail-soft" solid state modular array transmitter has been successfully demonstrated on the JPL Mesa Antenna Range. This integrated antenna and transmitter development is aimed at eliminating the use of the expensive, limited life X-band traveling wave tube amplifiers currently employed on deep space missions.

The antenna is composed of a near-field Cassegrainian reflector system[1,2] and a 32-element phased array feed, as shown in Fig. 1. 25 watts of power were injected into the radiating elements of the feed. This was accomplished with 32 three-quarter watt X-band solid state amplifiers each driving an element of the array. The amplifiers have a regulated dc to RF efficiency exceeding 25% and a gain over 15 dB. The antenna provides a directivity efficiency of about 65%.

Reflector System Design

The main reflector and the subreflector are confocal paraboloids having the same focal-length-to diameter ratio of 0.4. The magnification ratio of the reflector system (diameter of the main reflector to that of the subreflector) is 6.4. The tip of the array feed is about 24-wavelengths from the vertex of the subreflector, placing the subreflector in the near-field (tubular eam) region of the feed. The relatively small feed aperture is therefore magnified to the much larger main reflector aperture to produce high gain.

Feed Design

The feed, Fig. 2, is made up of a planar array consisting of 32 elements with a square grid arrangement, and is 0.51-m in diameter. Each array element is composed of a disc-on-rod (cigar) end-fire radiator with a square-cavity wave launcher, as shown in Fig. 3. Currently, the array element is linearly polarized, although it may readily be converted to circular polarization by redesigning the wave launcher. The separation between adjacent elements is 2-wavelengths, chosen to reduce the number of elements and the mutual-coupling effects and at the same time maintaining high antenna efficiency. The array element has been designed to have a relatively high directivity of 17 dB so as to keep the grating

*This paper presents the results of one phase of research carried out at the Jet Propulsion Laboratory, California Institute of Technology, under Contract No. NAS 7-100 sponsored by NASA.

lobe loss small (about 0.2 dB). Fig. 4 shows the E-plane far field pattern of the array feed. Also shown are two of the four grating lobes of the array.

A 32-way power divider made up of one 4-way divider and four 8-way dividers is used to feed the array elements. A solid state power amplifier for high power transmission and a line stretcher for vernier phase adjustment are connected between each element and each power divider output terminal. The power division, phasing, and amplification circuitry is shown in Fig. 5.

Solid-State Amplifier Design

The amplifier assembly consists of a three stage GaAs power FET microstrip configuration housed in an H-Frame module as illustrated in Fig. 6. Design requirements for the amplifier included an output level of 750 milliwatts at 8.415 GHz with a minimum gain of 15 dB and power added efficiency greater than 25%. FET devices selected for the three stage amplifier are rated at 1/4, 1/2 and 1 watt respectively, each operating at a power derated level for reliability. RF coupling and interstage matching for transistors are provided by six-single pole microstrip transmission line networks designed on Duroid laminate. An output load isolator is included to protect the final FET from large load variations. To maximize efficiency, each stage is biased to operate 1.5 dB into gain compression. Drain and gate supply voltages are +5.5 volts and -5.0 volts respectively with a total DC input power of 2.9 watts maximum.

Test results of the 34 amplifier modules as fabricated indicated the following: 1) power output ranged from 700 to 800 milliwatts; 2) regulated dc to RF efficiency ranged from 25 to 30 percent; 3) 1 dB bandwidth ranged from 200 to 400 MHz; 4) small signal gain exceeded 20 dB, and compressed to 15.7 dB at the operating point; and 5) relative phase among the 34 units spread across 120 degrees. By using a built in fixed 3 bit phase shifter and the variable line stretchers the relative phase difference among the 32 amplifiers at the final array assembly test was 2.5 degrees, one sigma; which will contribute less than 0.01 dB loss to the phase efficiency.

Antenna Radiation Pattern

Fig. 7 shows a typical far field pattern of the antenna. There are practically no differences between the antenna patterns before and after the insertion of the amplifiers into the feed circuitry when the amplitude and phase distributions of the signals feeding into the array elements are correctly adjusted.

References

1. W. D. Fitzgerald, 1971 Lincoln Laboratory Report 484.
2. Kenneth Woo and Paul Cramer, Jr., IEEE AP-S International Symposium Digest, pp. 323-325, 1976.

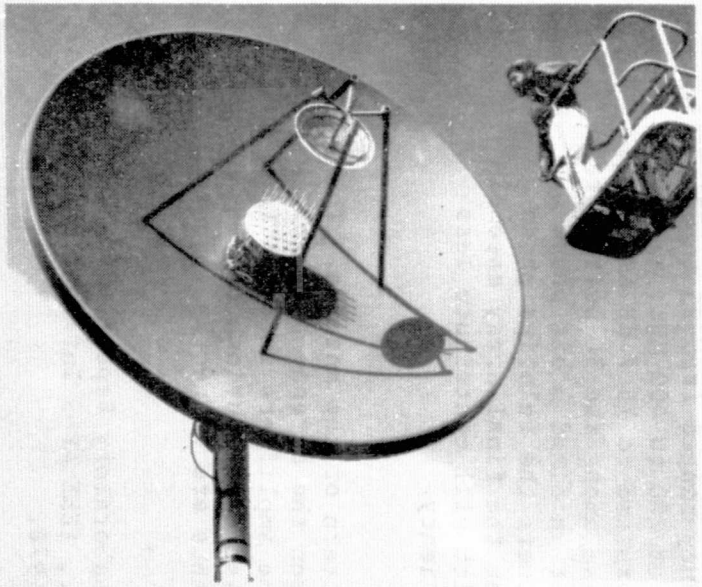

FIGURE 1. X-BAND HIGH-GAIN ANTENNA WITH SOLID-STATE TRANSMITTER

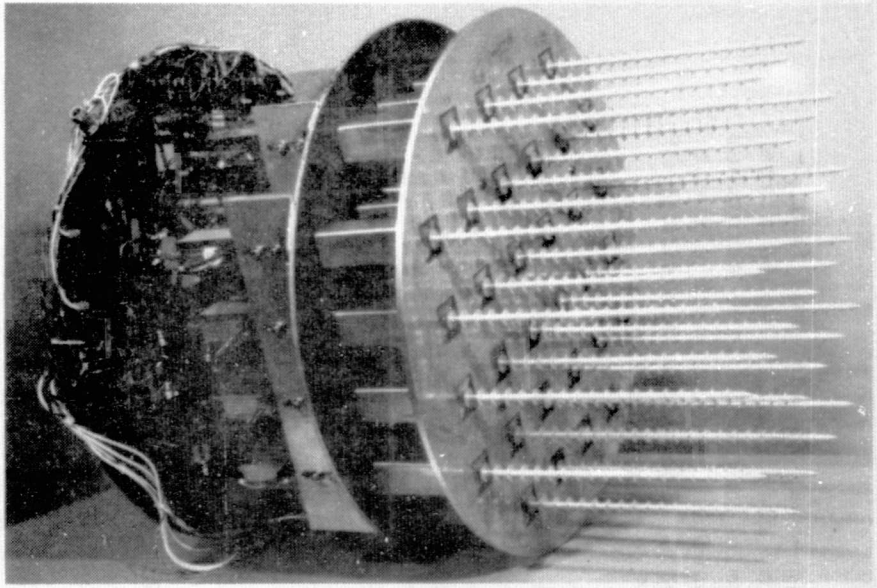

FIGURE 2. FEED DESIGN

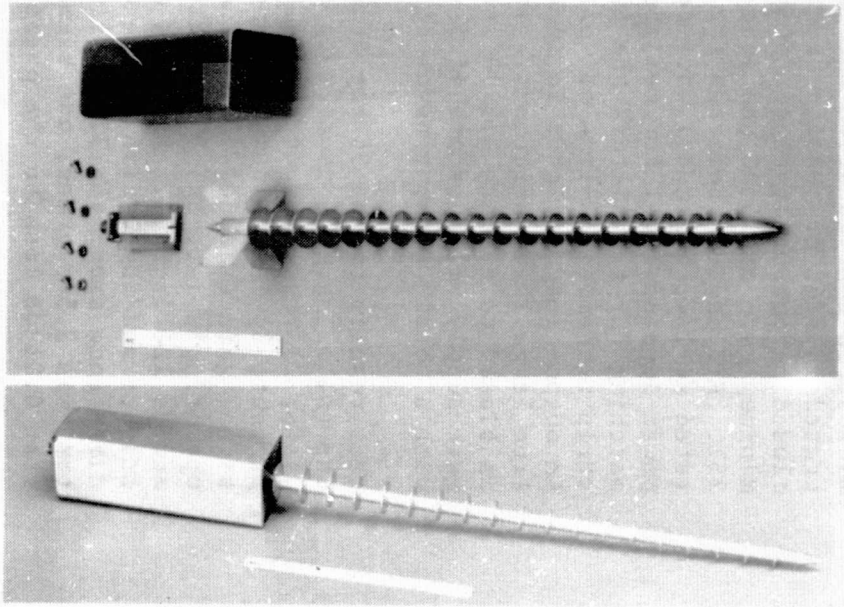

FIGURE 3. ARRAY ELEMENT DESIGN

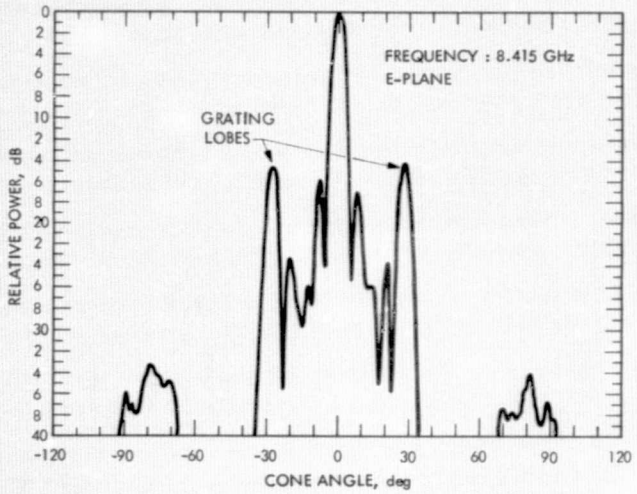

FIGURE 4. ARRAY FEED FAR FIELD PATTERN, MEASURED

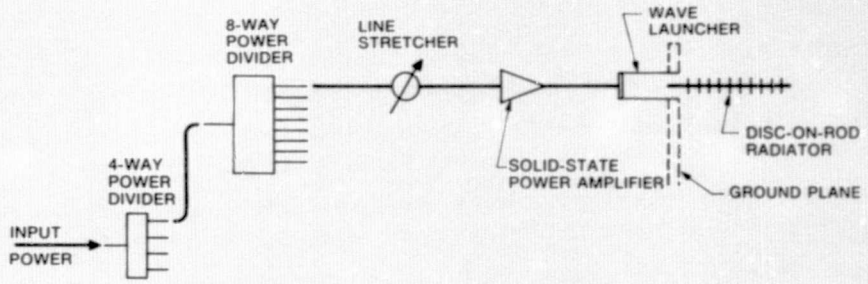

FIGURE 5. POWER DIVISION, PHASING, AND AMPLICATION CIRCUITRY

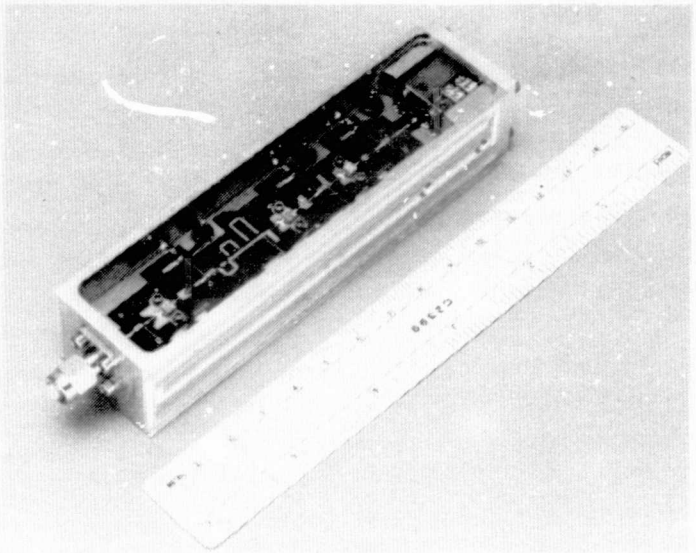

FIGURE 6. AMPLIFIER DESIGN

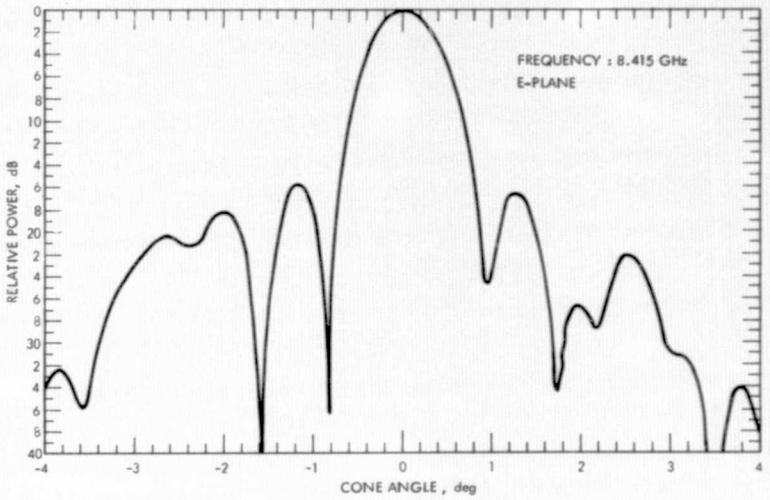

FIGURE 7. ANTENNA FAR FIELD PATTERN, MEASURED